

*Galactic
Chemical
Evolution
with
Radioactive
Isotopes*

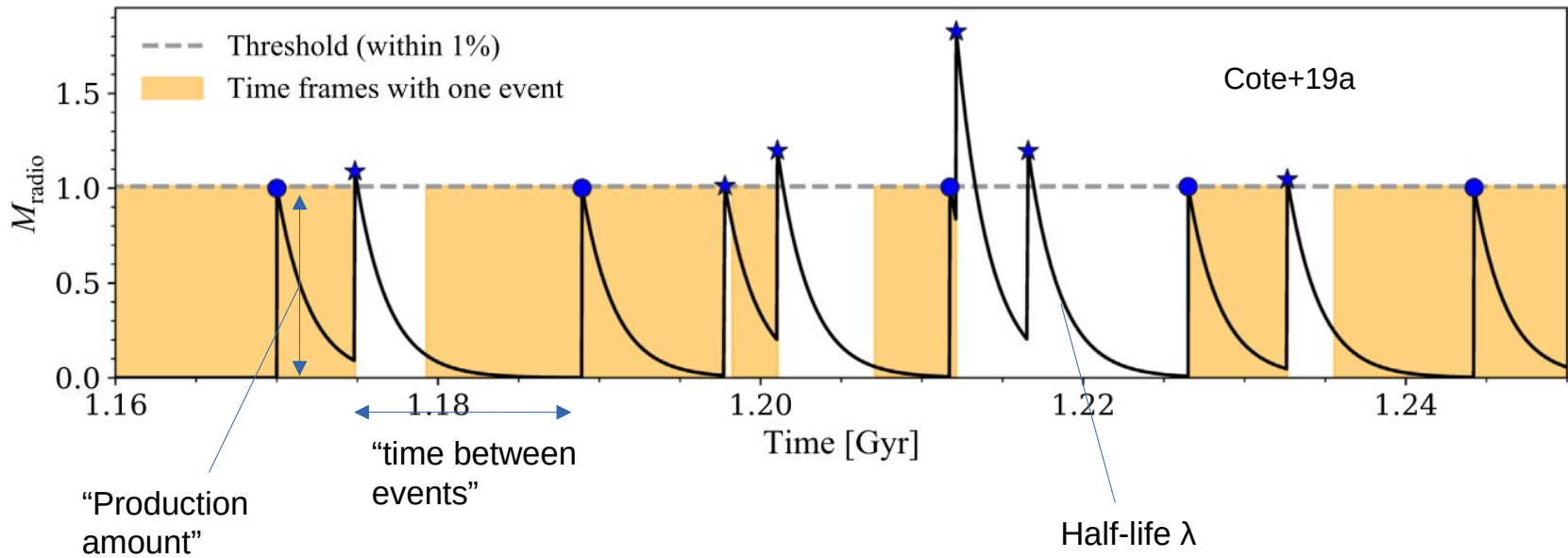
Benjamin Wehmeyer

>Univ of Wroclaw, Poland

>Konkoly Observatory, Hungary

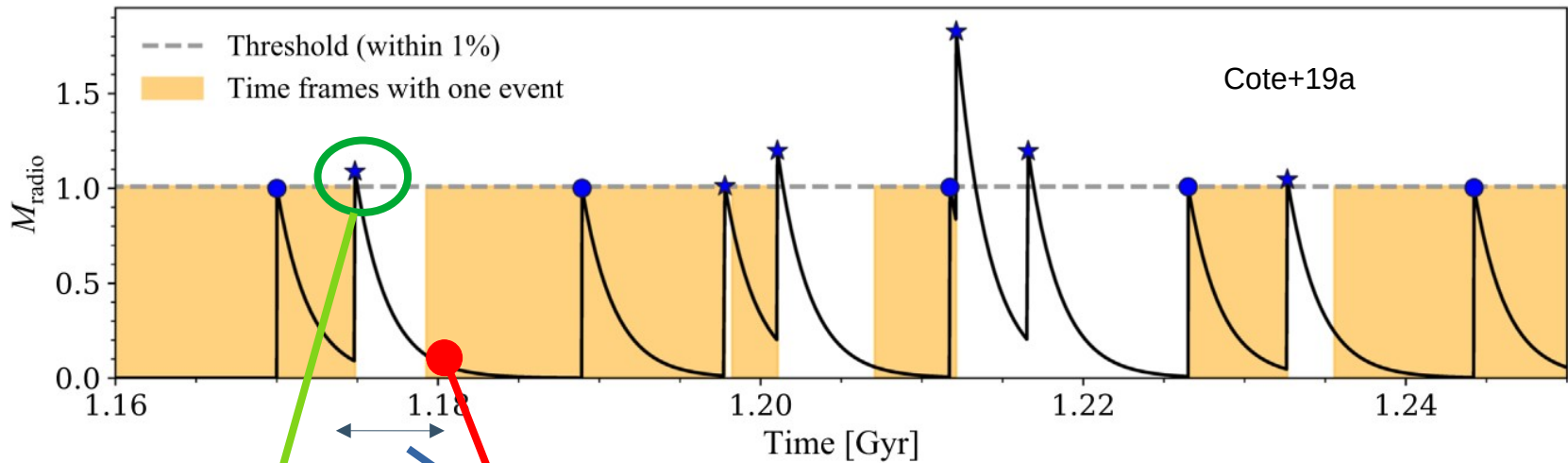
>Univ of Hertfordshire, UK

Imagine an arbitrary astrophysical source of radioactive isotopes:



Production value, observed value, elapsed time:
If you know two, you may draw conclusions about the third!

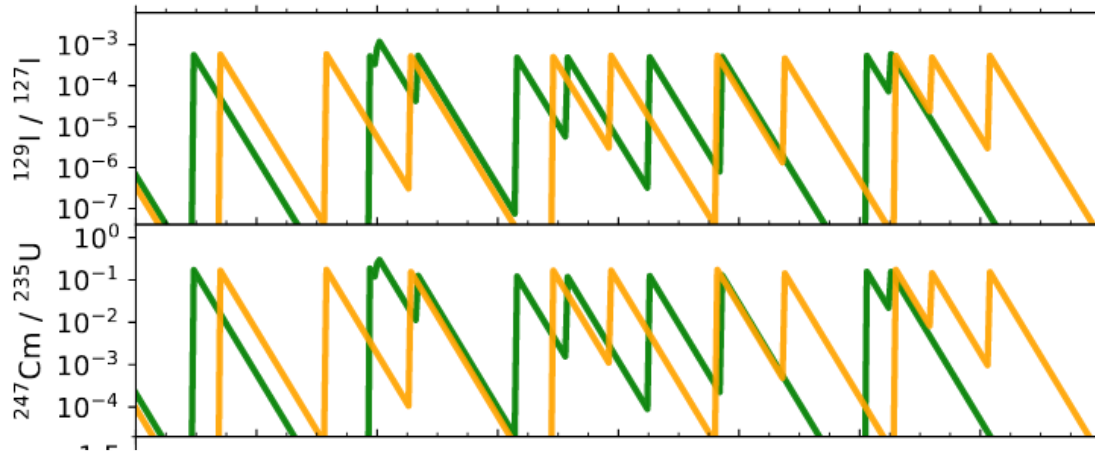
Imagine an arbitrary astrophysical source of radioactive isotopes:



Production value, observed value, elapsed time:

If you know two, you may draw conclusions about the third!

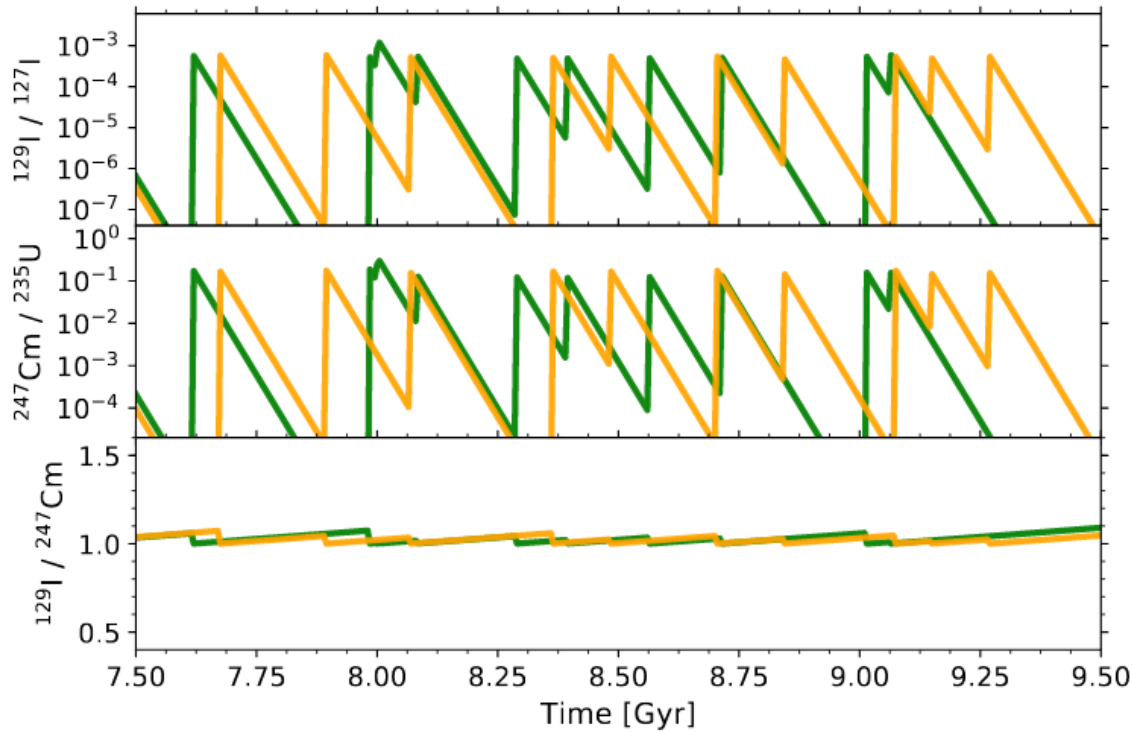
If you build the ratio of a combination of two **great, special** isotopes...



Côté+,
2021Science 371,
945C

Produced exclusively by
the r-process...
...and have very similar
half-lives...

If you build the ratio of a combination of two **great, special** isotopes...



Côté+,
2021Science 371,
945C

Produced exclusively by
the r-process...
...and have very similar
half-lives...
You'll end up with a **LINE!**

If you build the ratio of a combination of two **great, special** isotopes...

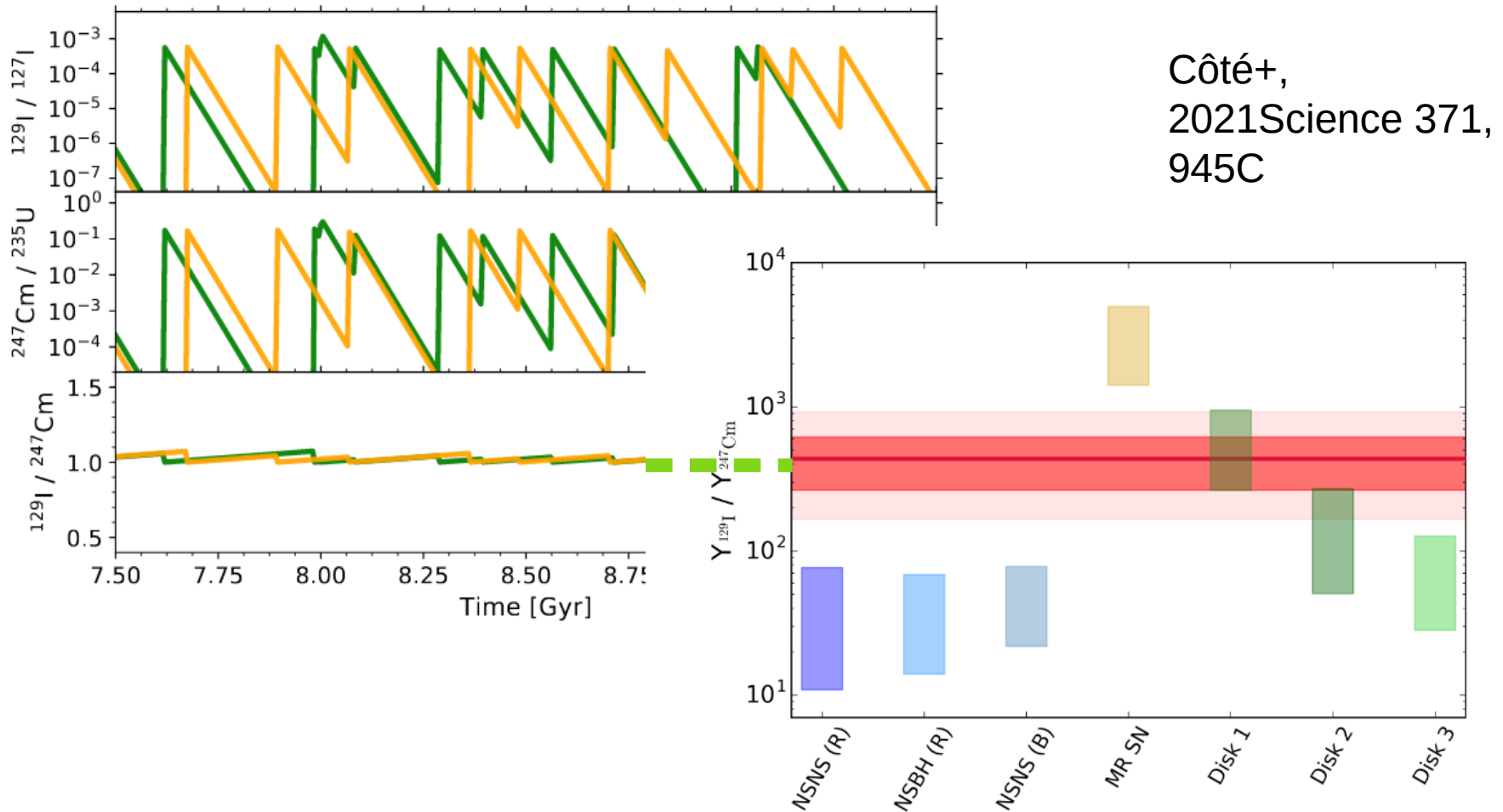


Fig. 2. $^{129}\text{I} / ^{247}\text{Cm}$ abundance ratios predicted by our theoretical r -process models (see Methods section). The red horizontal line and horizontal bands show the meteoritic ratio along with its 1σ and 2σ uncertainty (see Methods section).

If you build the ratio of a combination of two **great, special** isotopes...

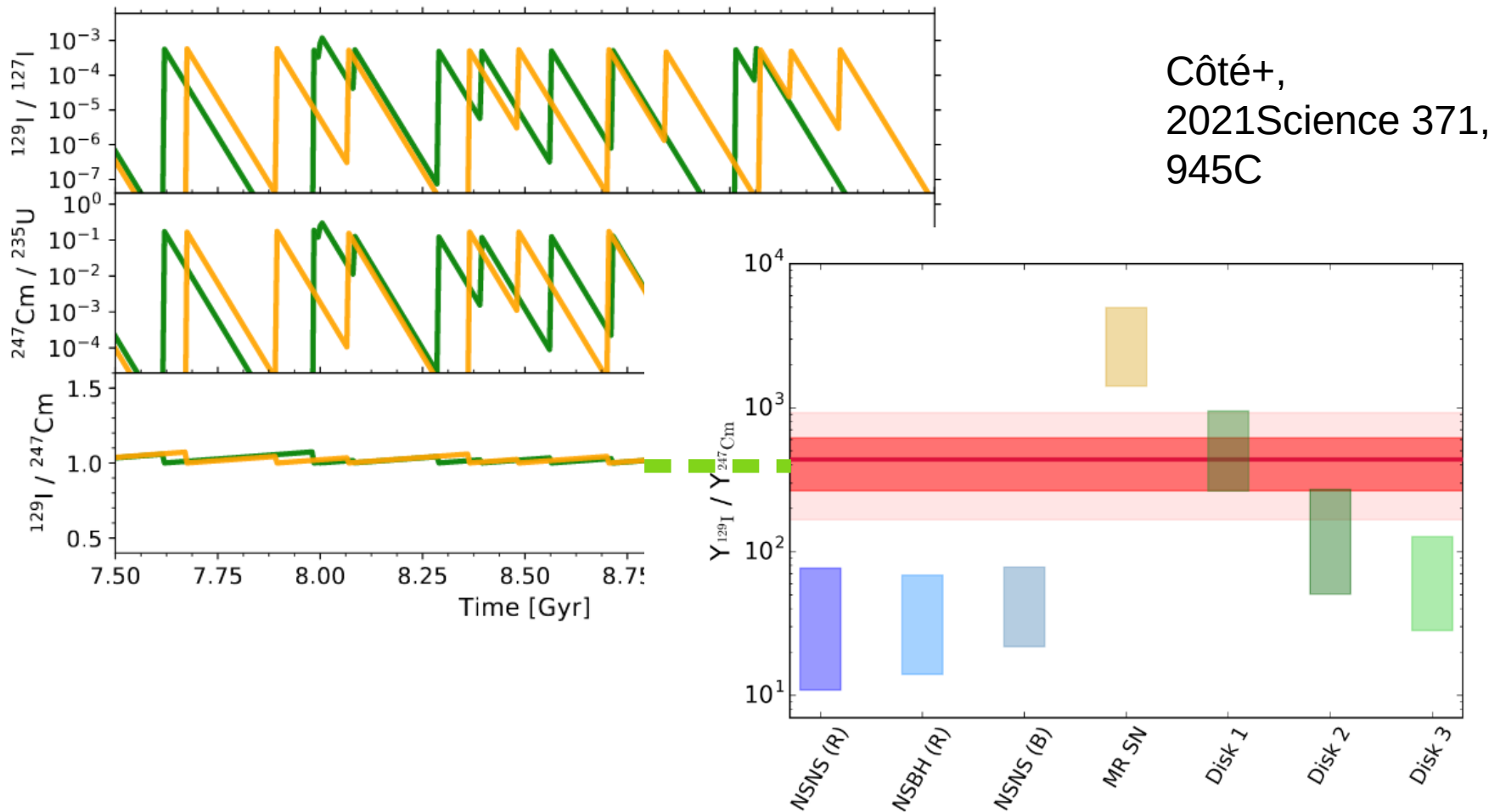


Fig. 2. $^{129}\text{I}/^{247}\text{Cm}$ abundance ratios predicted by our theoretical r -process models (see Methods section). The red horizontal line and horizontal bands show the meteoritic ratio along with its

...allowing you to directly probe the yield ratios of the last r -process event!!!!

Why does this work?

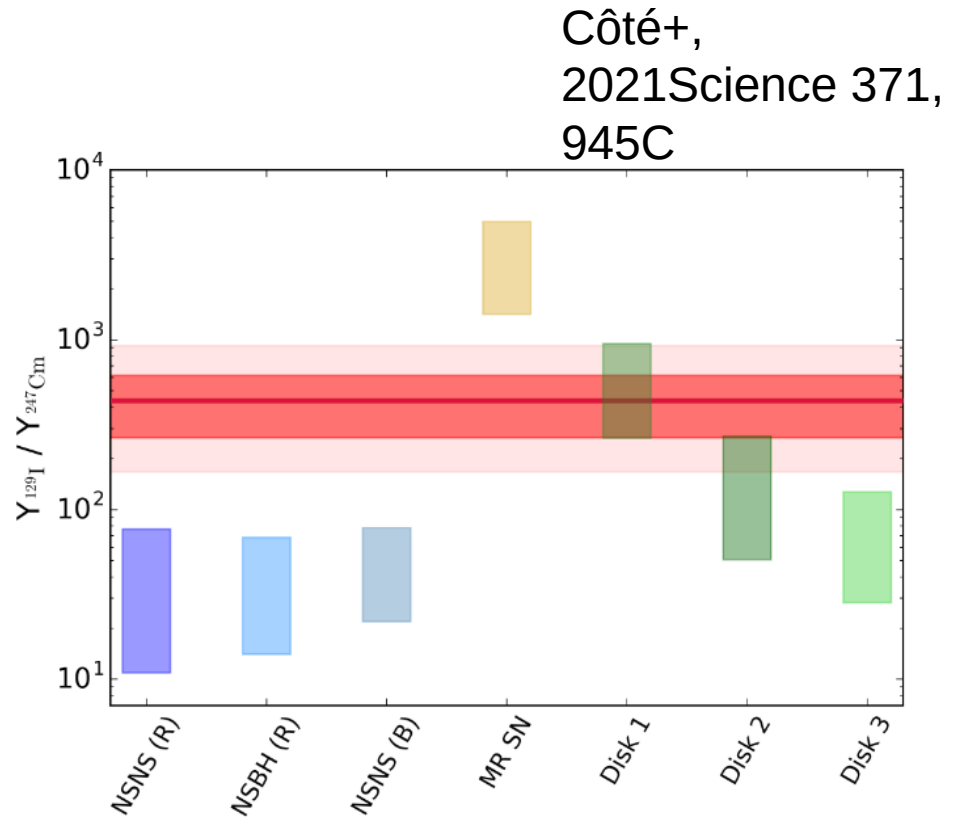
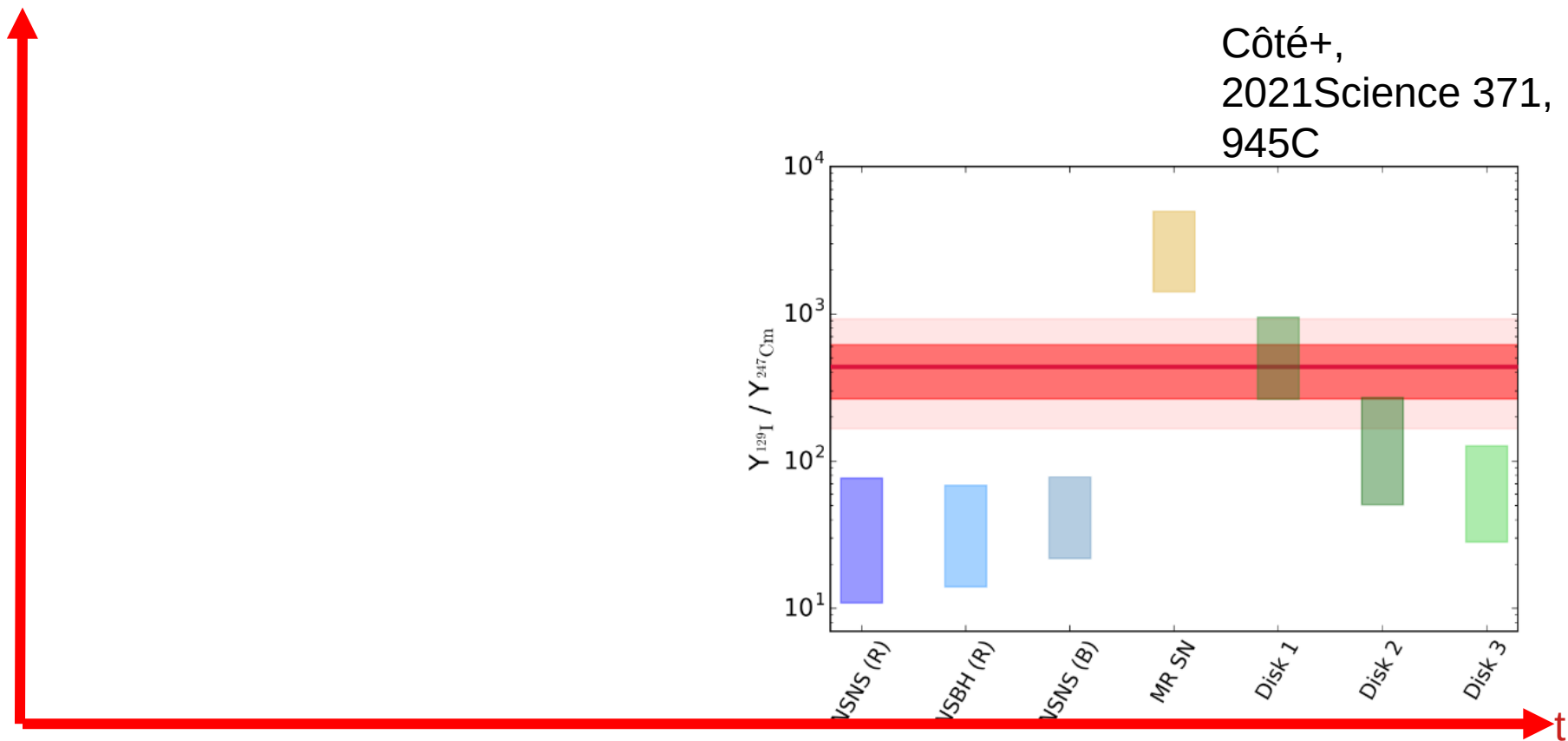


Fig. 2. $^{129}\text{I}/^{247}\text{Cm}$ abundance ratios predicted by our theoretical r -process models (see Methods section). The red horizontal line and horizontal bands show the meteoritic ratio along with its 1σ and 2σ uncertainty (see Methods section).

Why does this work?



Let's look at the evolution before the formation of the Solar system.

Fig. 2. $^{129}\text{I}/^{247}\text{Cm}$ abundance ratios predicted by our theoretical r -process models (see Methods section). The red horizontal line and horizontal bands show the meteoritic ratio along with its 1σ and 2σ uncertainty (see Methods section).

Why does this work?

...because **even if any other r-process sources have contributed to the ratio before,**

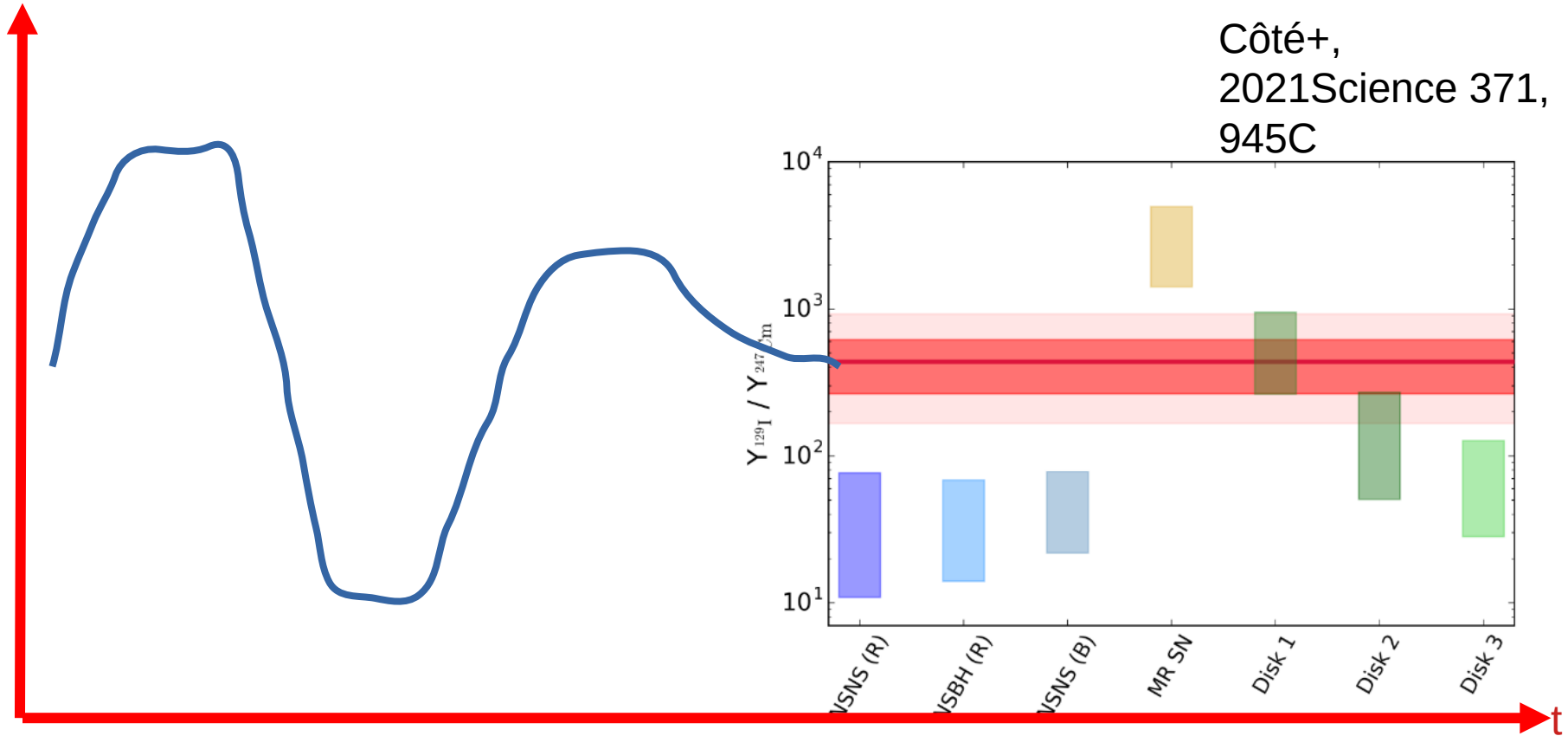
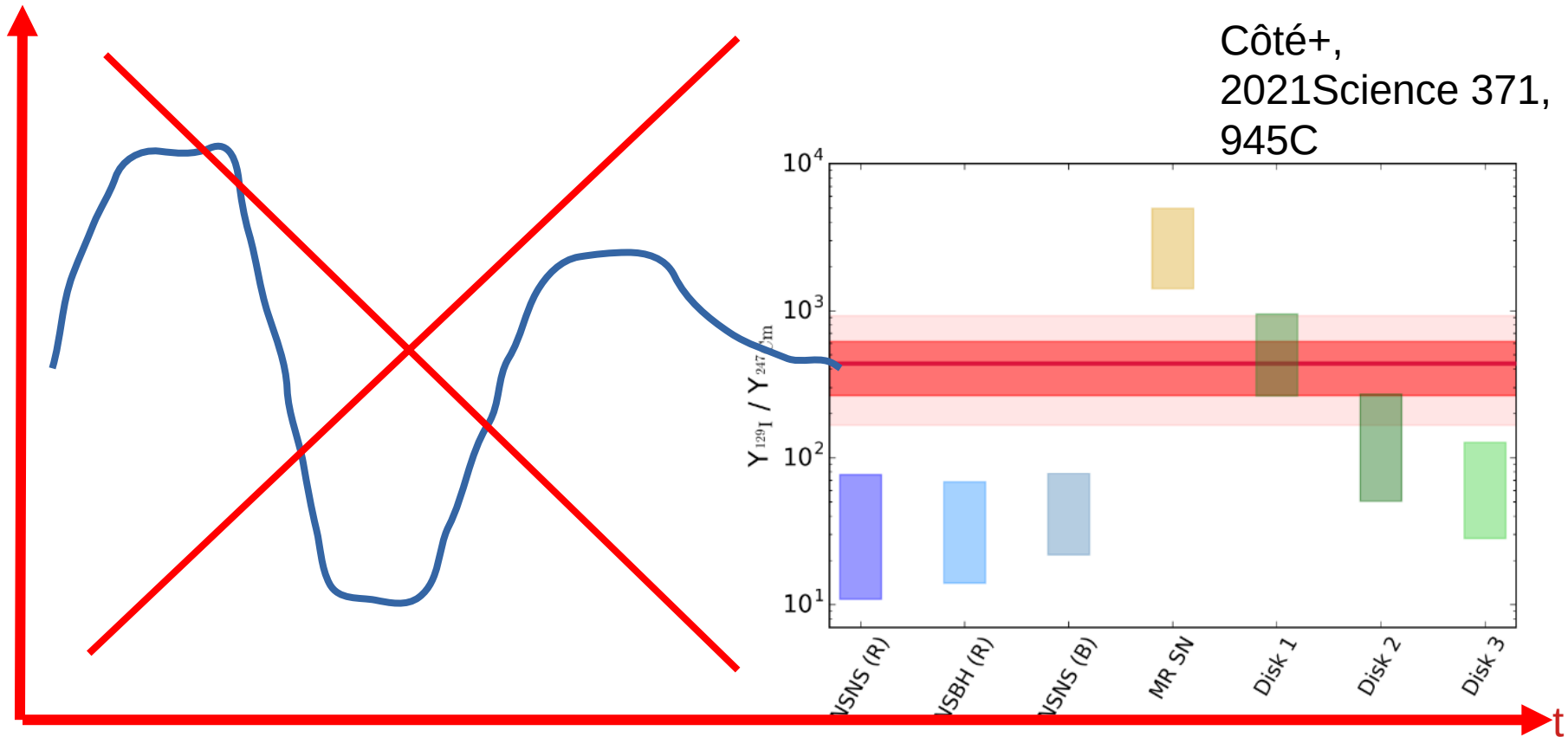


Fig. 2. $^{129}\text{I}/^{247}\text{Cm}$ abundance ratios predicted by our theoretical *r*-process models (see Methods section). The red horizontal line and horizontal bands show the meteoritic ratio along with its 1σ and 2σ uncertainty (see Methods section).

Why does this work?

...because **even if any other r-process sources have contributed to the ratio before, their contribution is gone!**



Côté+,
2021Science 371,
945C

Fig. 2. $^{129}\text{I} / ^{247}\text{Cm}$ abundance ratios predicted by our theoretical *r*-process models (see Methods section). The red horizontal line and horizontal bands show the meteoritic ratio along with its 1σ and 2σ uncertainty (see Methods section).

...this enables us to precisely study the LAST r-process event that contributed to the Solar system!

If you look at the whole Galaxy, however,
And have variable delay times (NSMs)...

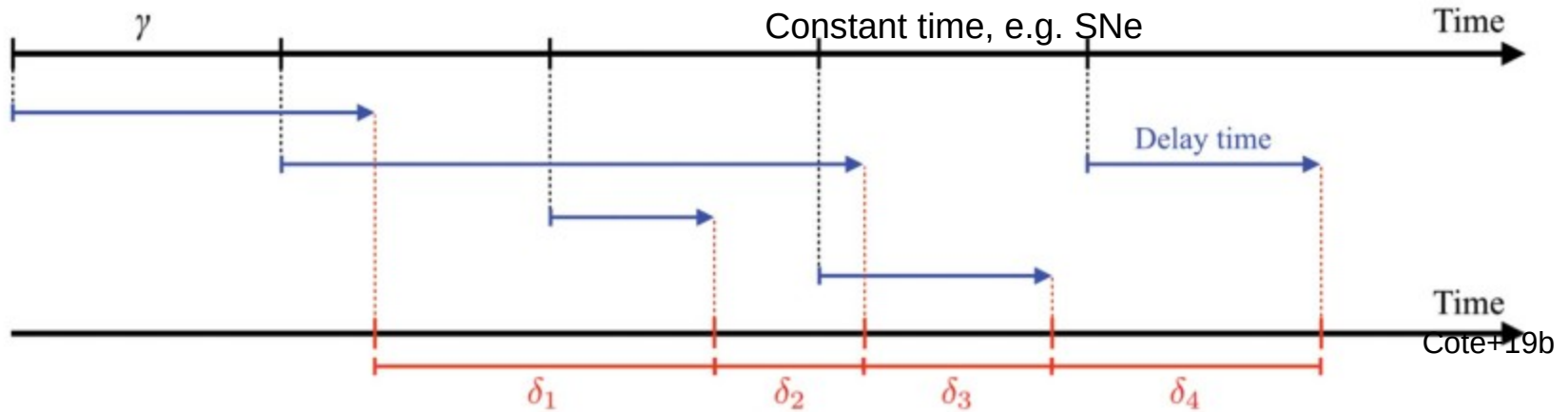


Figure 2. Visualization of the key parameters involved in our Monte Carlo calculations. Here γ is the constant time interval between the formation of two progenitors. The delay times (blue arrows) represent the time intervals between the formation of the progenitors and their associated enrichment event. Those delay times are randomly sampled from an input DTD function. The different δ values are the time intervals between two consecutive enrichment events, regardless of the formation time of the progenitors. This means that δ cannot have negative values.

If you look at the whole Galaxy, however,
And have variable delay times (NSMs)...

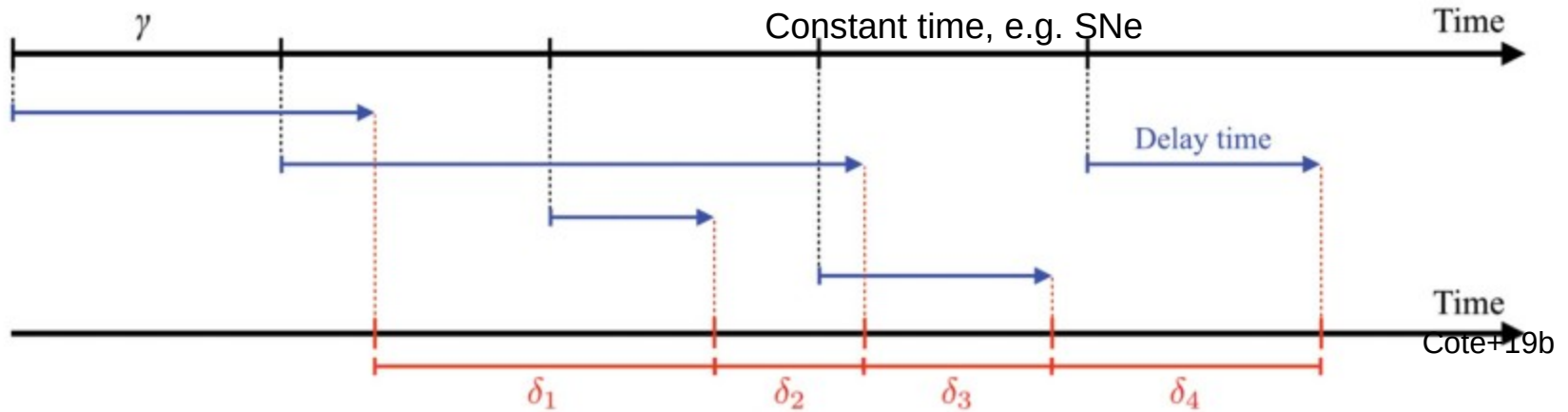
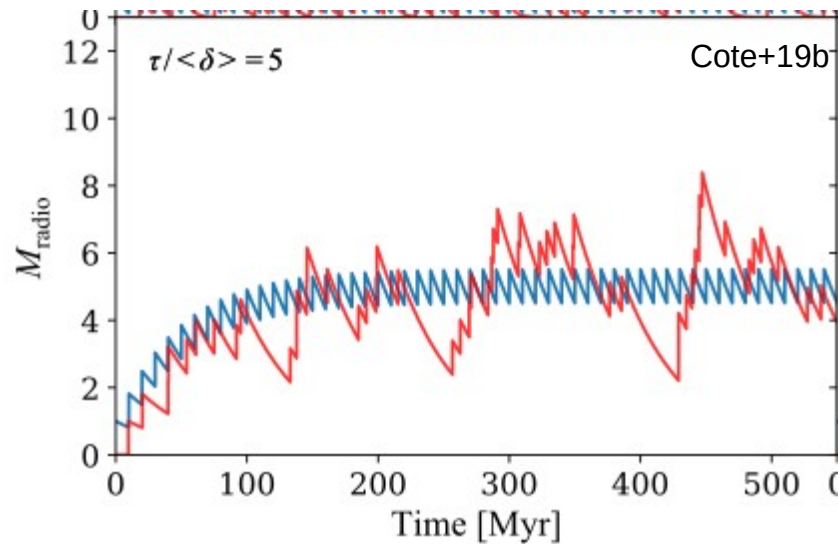


Figure 2. Visualization of the key parameters involved in our Monte Carlo calculations. Here γ is the constant time interval between the formation of two progenitors. The delay times (blue arrows) represent the time intervals between the formation of the progenitors and their associated enrichment event. Those delay times are randomly sampled from an input DTD function. The different δ values are the time intervals between two consecutive enrichment events, regardless of the formation time of the progenitors. This means that δ cannot have negative values.

...this this tends to extend the steady-state value...



...leading rather to a *spectrum* of abundances:

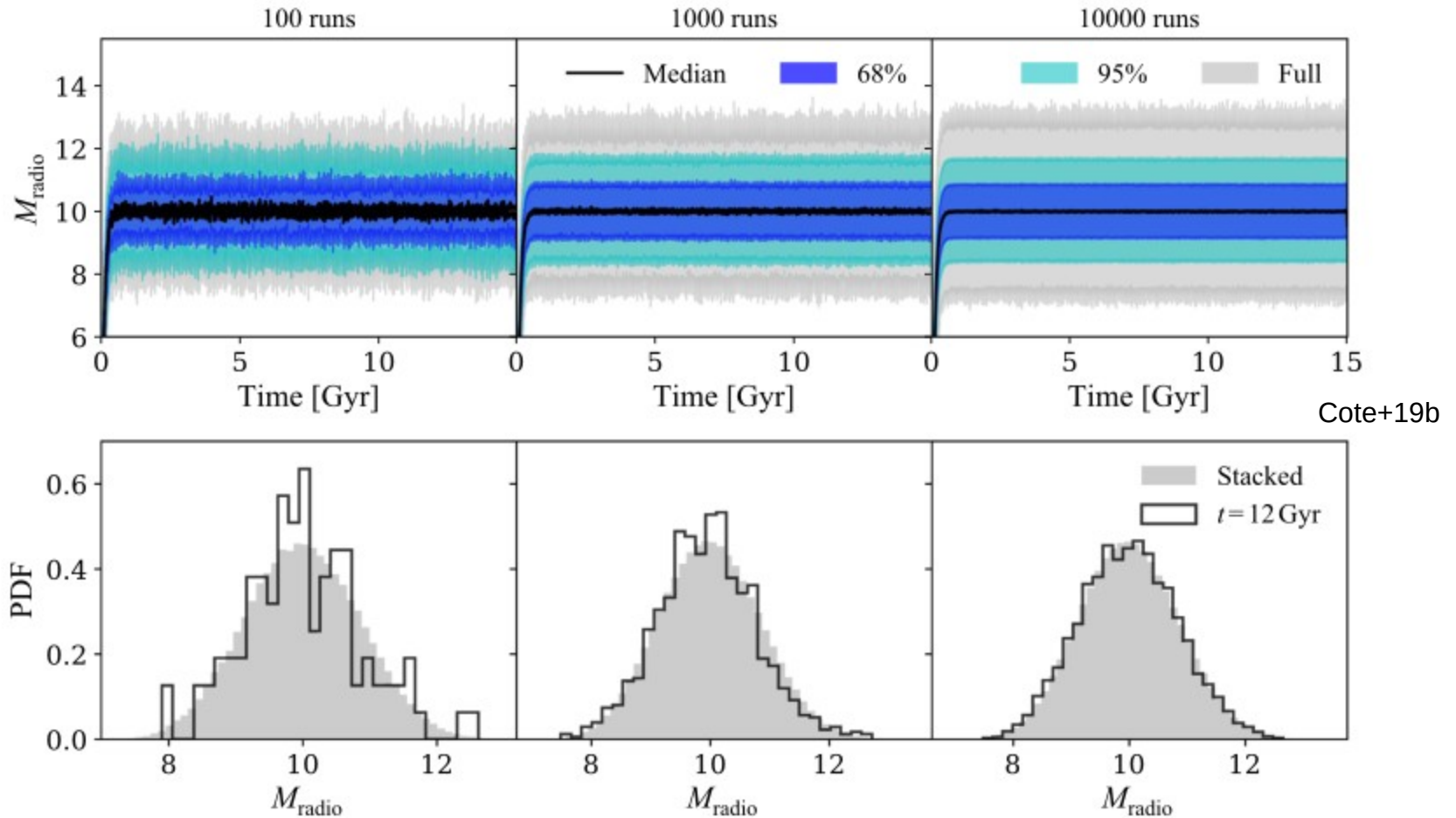


Figure 3. Top panels: evolution of the median and 68% and 95% confidence levels of the mass of radionuclei (M_{radio}) as a function of time using Monte Carlo calculations with 100, 1000, and 10,000 runs (from left to right), with $\gamma = 10$ Myr and the 3–50 Myr box DTD function. The gray shaded area represents the maximum and minimum values reached during the calculations. Bottom panels: distribution of predicted M_{radio} at 12 Gyr (black histograms) for the calculations with 100, 1000, and 10,000 runs (from left to right). The gray histograms show the distribution of M_{radio} when all time steps between 12 and 14 Gyr are stacked together to improve the statistics.

...leading rather to a *spectrum* of abundances:

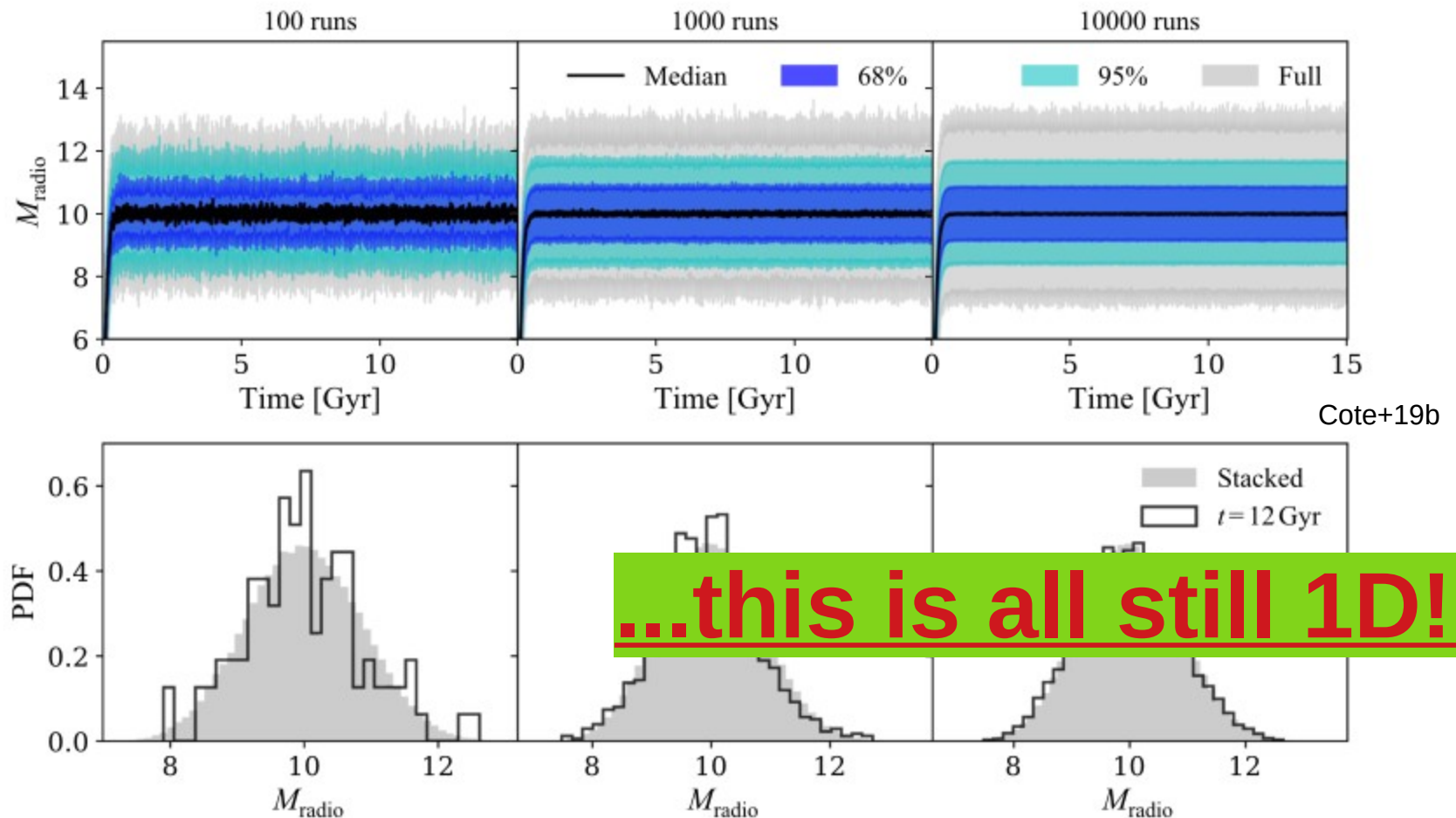
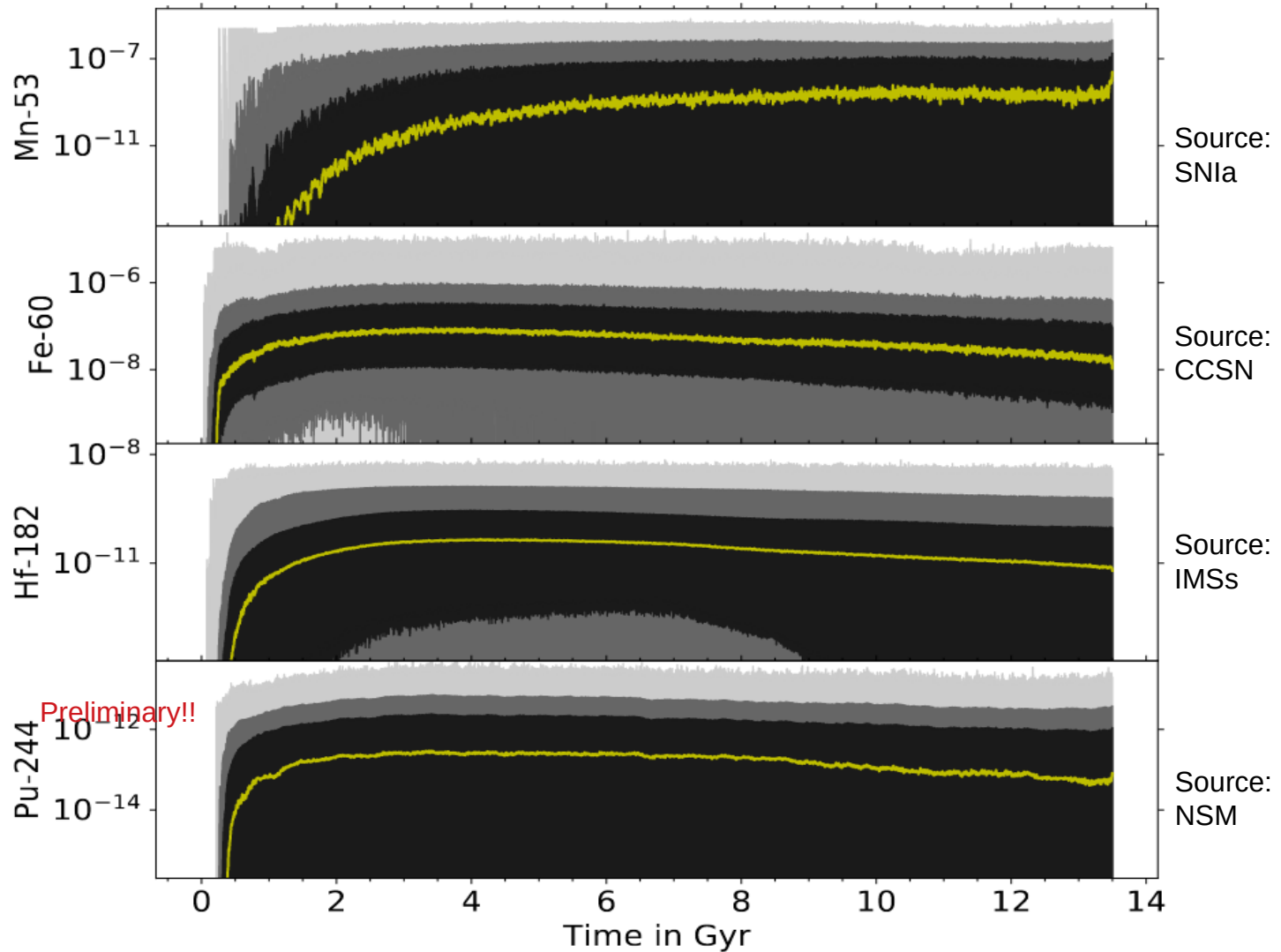


Figure 3. Top panels: evolution of the median and 68% and 95% confidence levels of the mass of radionuclei (M_{radio}) as a function of time using Monte Carlo calculations with 100, 1000, and 10,000 runs (from left to right), with $\gamma = 10$ Myr and the 3–50 Myr box DTD function. The gray shaded area represents the maximum and minimum values reached during the calculations. Bottom panels: distribution of predicted M_{radio} at 12 Gyr (black histograms) for the calculations with 100, 1000, and 10,000 runs (from left to right). The gray histograms show the distribution of M_{radio} when all time steps between 12 and 14 Gyr are stacked together to improve the statistics.

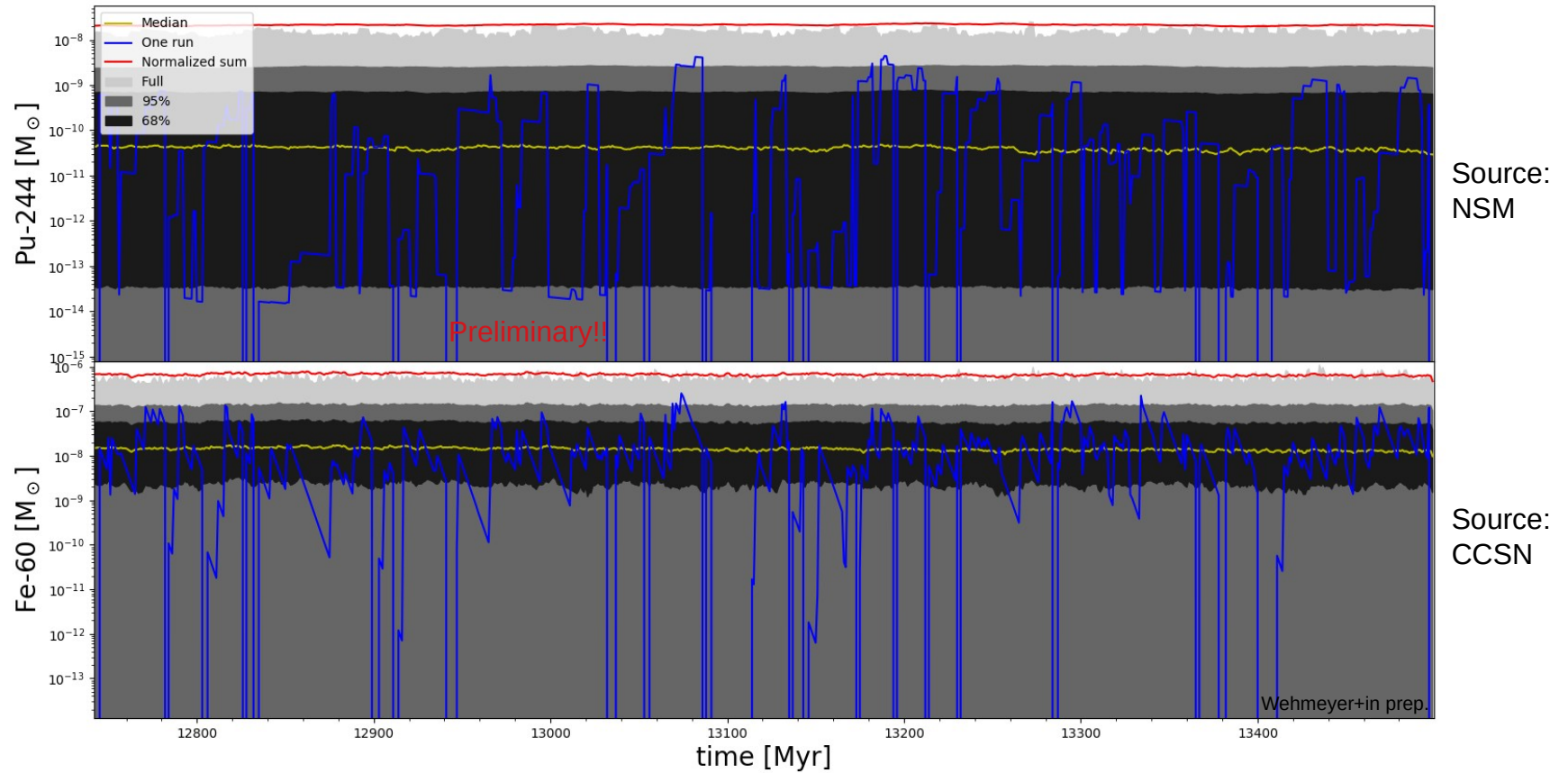
Moving to 3D this gets even more complicated!



- All follow the Galactic SFH
Yellow: median, grey scales: statistics

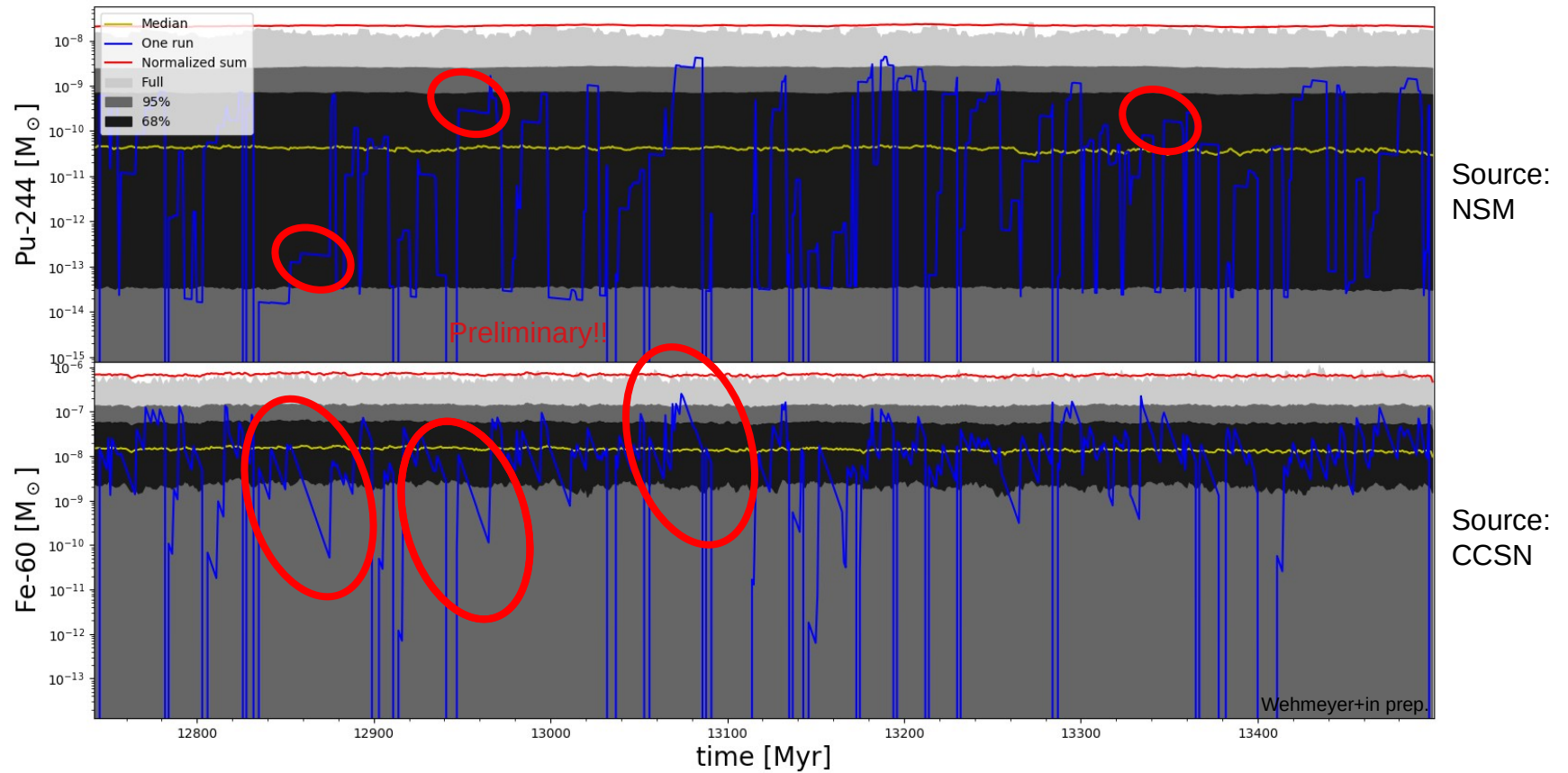
Moving to 3D this gets even more complicated!

Zoom in



Yellow: median, grey scales: statistics
Blue: Single sub-cell of the 3D simulation

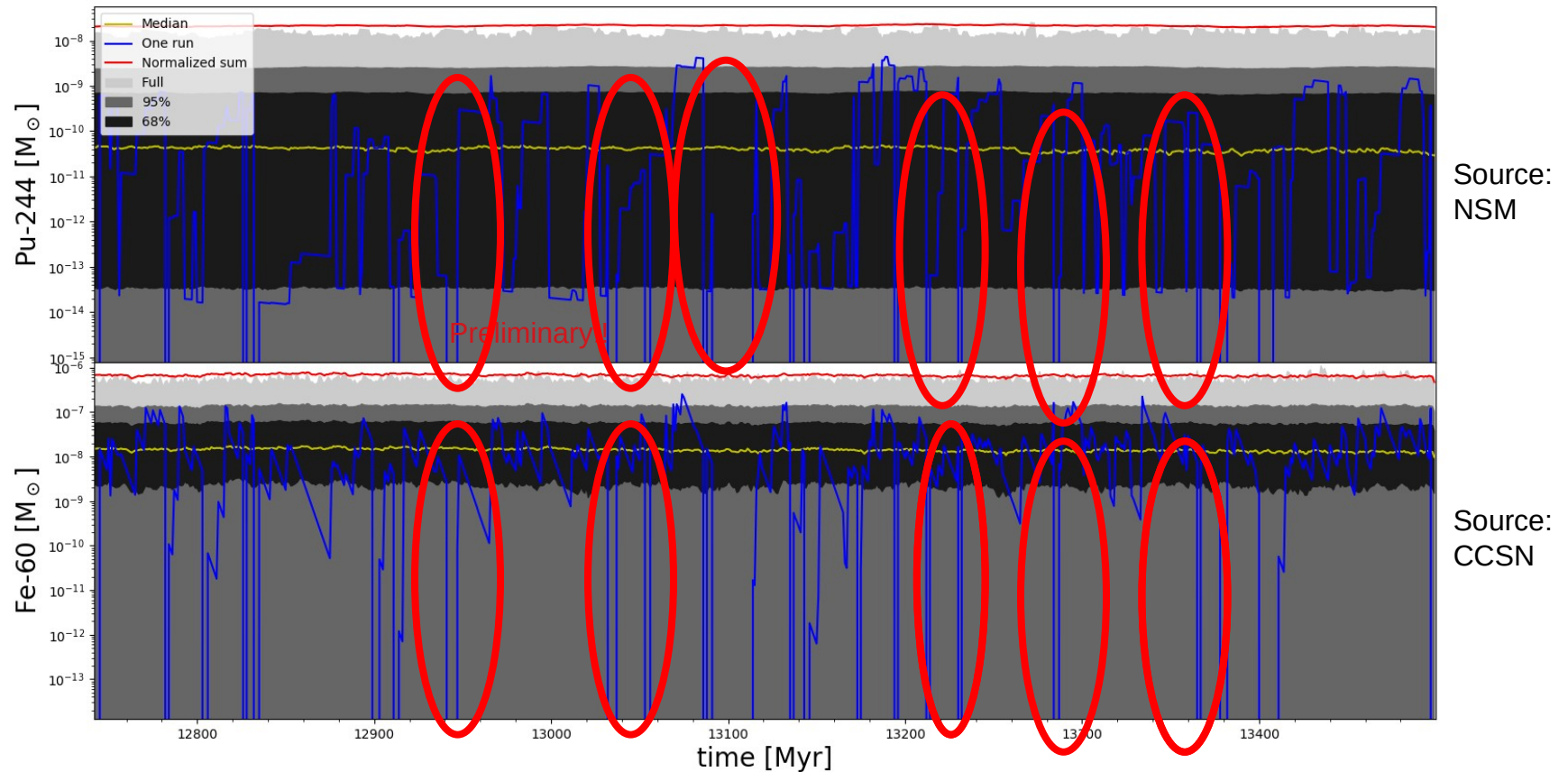
Moving to 3D this gets even more complicated!



Remarks:

- Radioactive decay is visible in single cells (between nucl events)

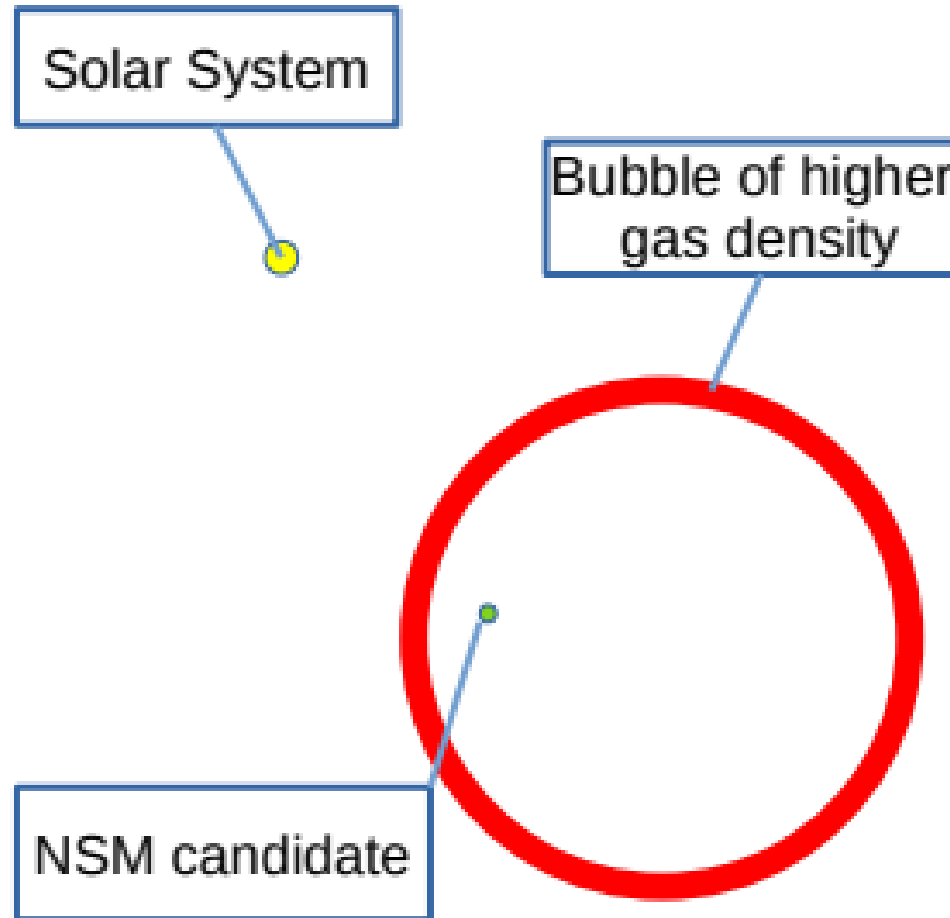
Moving to 3D this gets even more complicated!



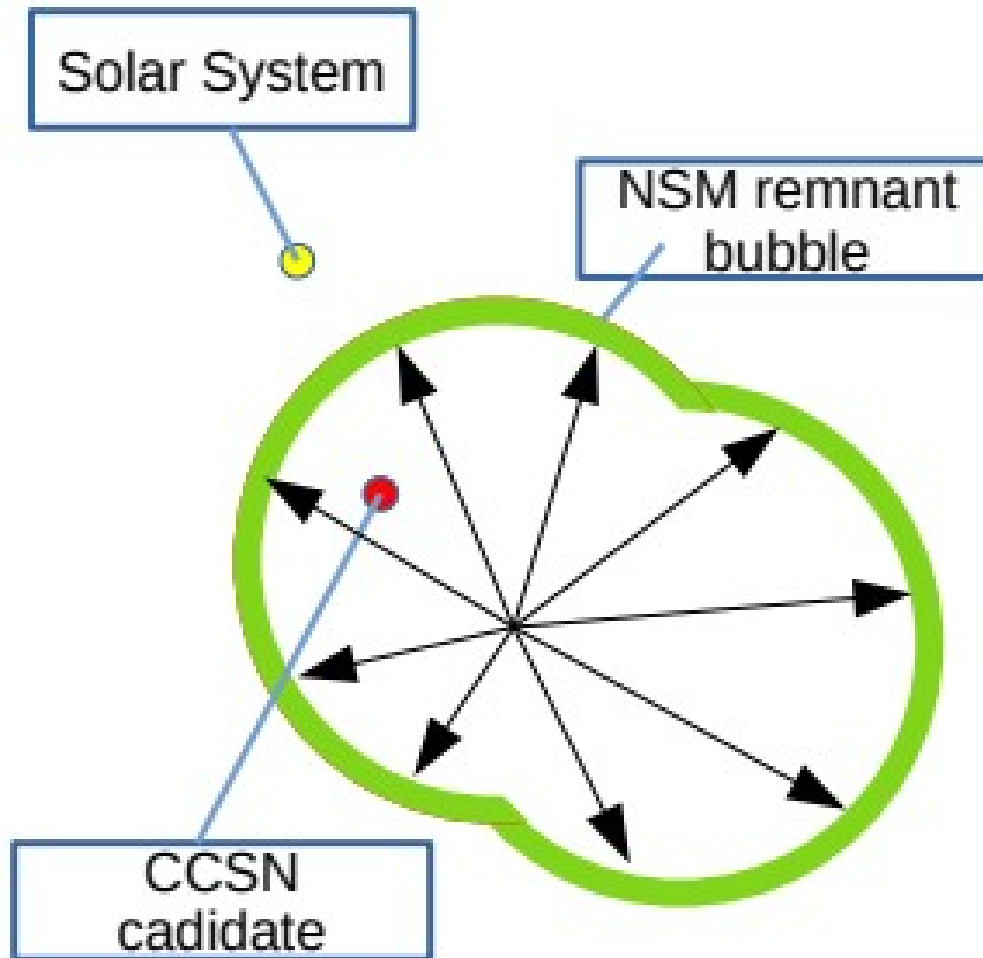
Remarks:

- Radioactive decay is visible in single cells (between nucl events)
- This is often hidden behind the SN blast wave effect
- Pu-244 & Fe-60 always seem to appear **simultaneously**

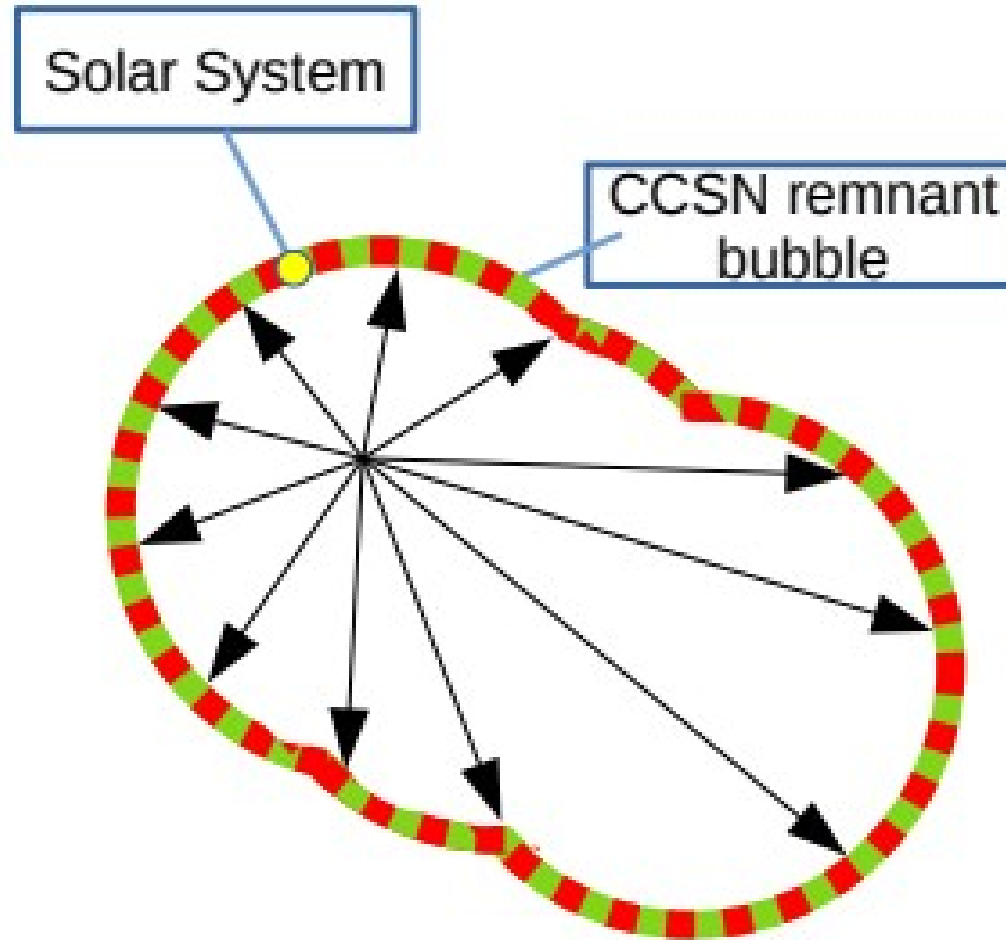
What happens if NSM ejecta get “bulldozed” by CCSN bubbles?



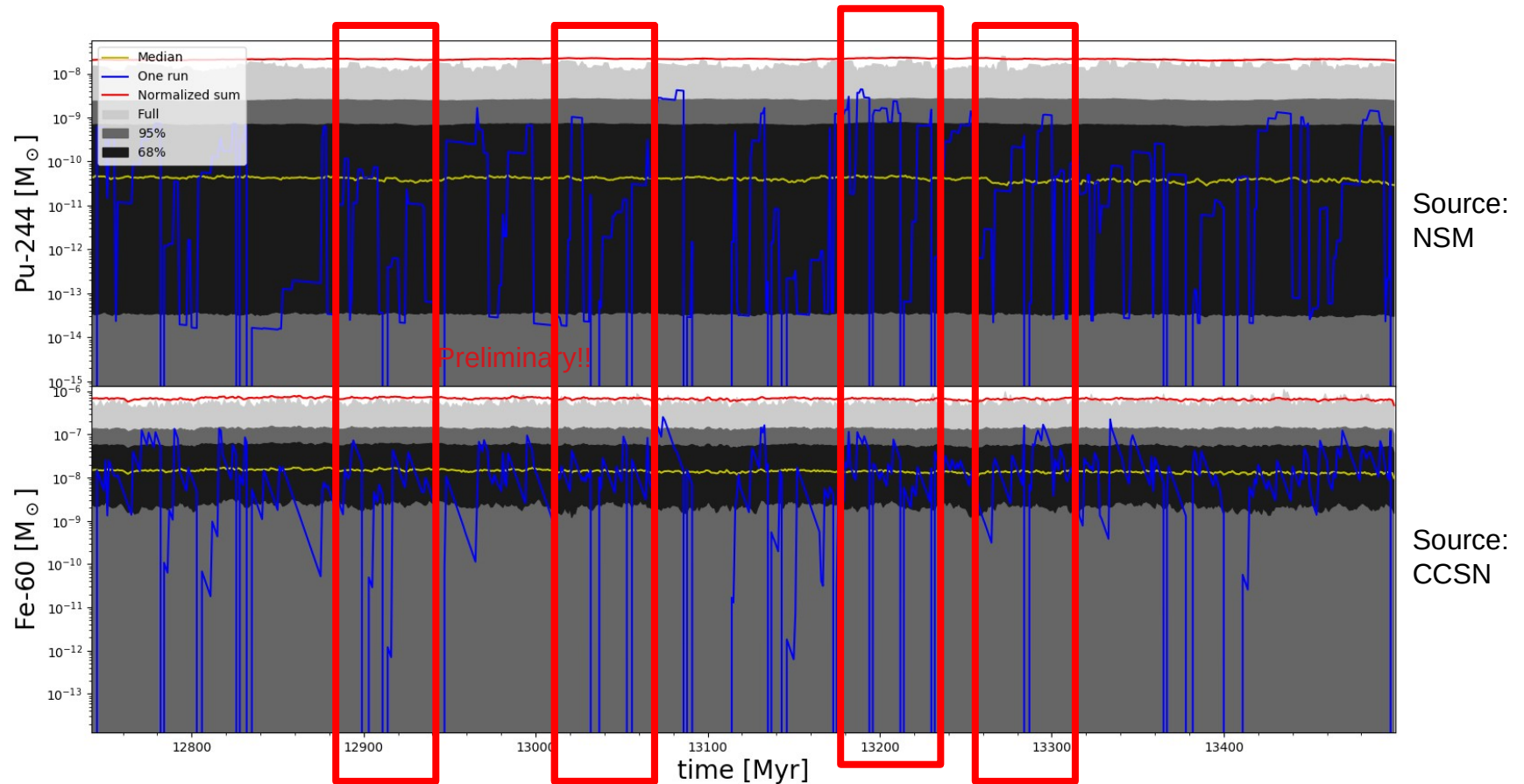
What happens if NSM ejecta get “bulldozed” by CCSN bubbles?



What happens if NSM ejecta get “bulldozed” by CCSN bubbles?

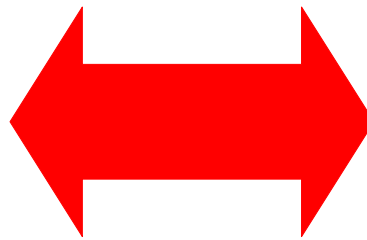
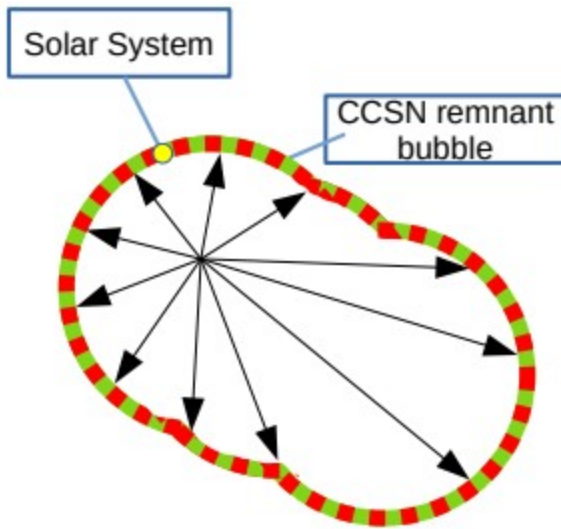


Moving to 3D this gets even more complicated!

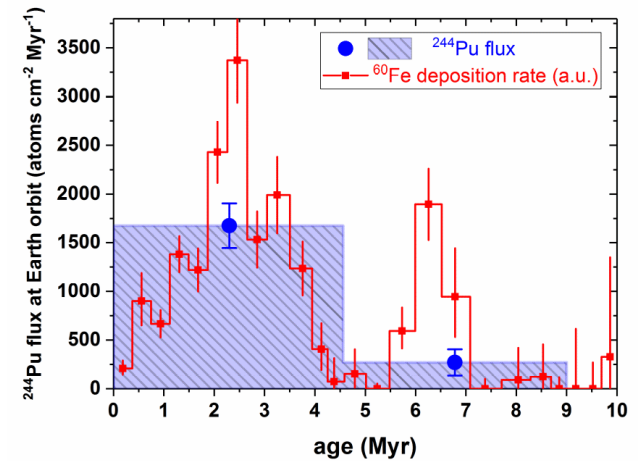


Remarks:

- Radioactive decay is visible in single cells (between nucl events)
- This is hidden behind the SN blast wave effect
- Pu-244 & Fe-60 always seem to appear **simultaneously**



^{244}Pu flux vs ^{60}Fe flux



Unknown site of actinide nucleosynthesis -- Wallner -- Trento 1-5 July 2019

...confirms what is seen
in deep-sea sediments:
Fe-60 and Pu-244 seem to
arrive simultaneously on Earth!

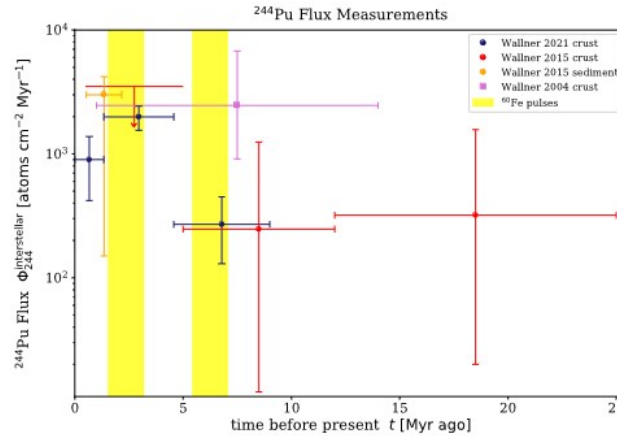
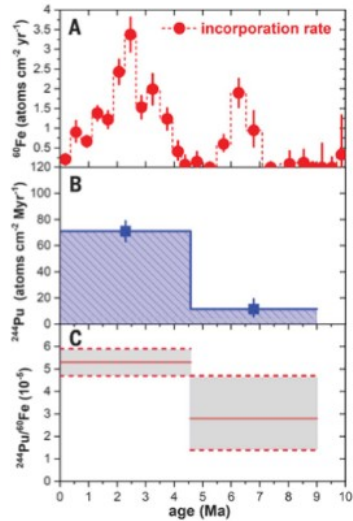
Solar System

See also Rebecca's talk this morning:

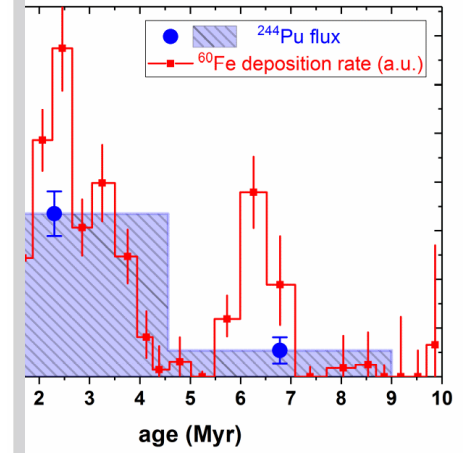
^{244}Pu flux vs ^{60}Fe flux

Actinide observables: ^{60}Fe and ^{244}Pu in Fe-Mn crusts

Wallner+2021

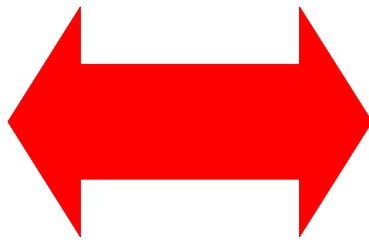
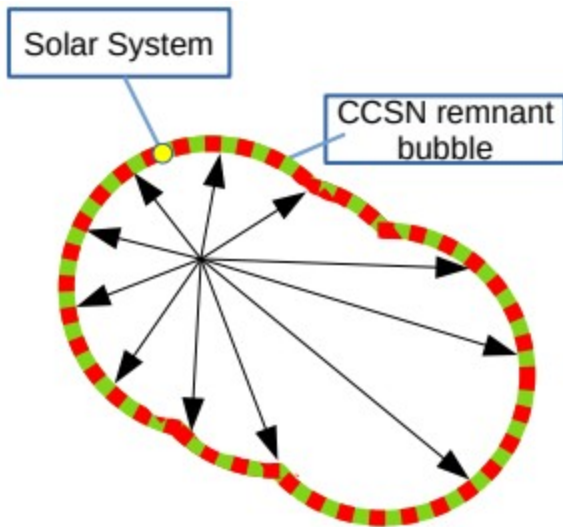


Wang, Clark, Ellis, Ertel, Fields, Fry, Liu, Miller, Surman, ApJ 2021

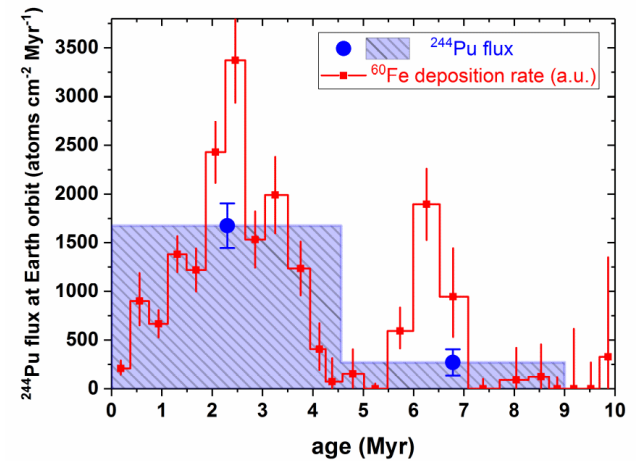


leosynthesis -- Wallner -- Trento 1-5 July 2019

Fe-60 and Pu-244 seem to arrive simultaneously on Earth!



^{244}Pu flux vs ^{60}Fe flux



Unknown site of actinide nucleosynthesis -- Wallner -- Trento 1-5 July 2019

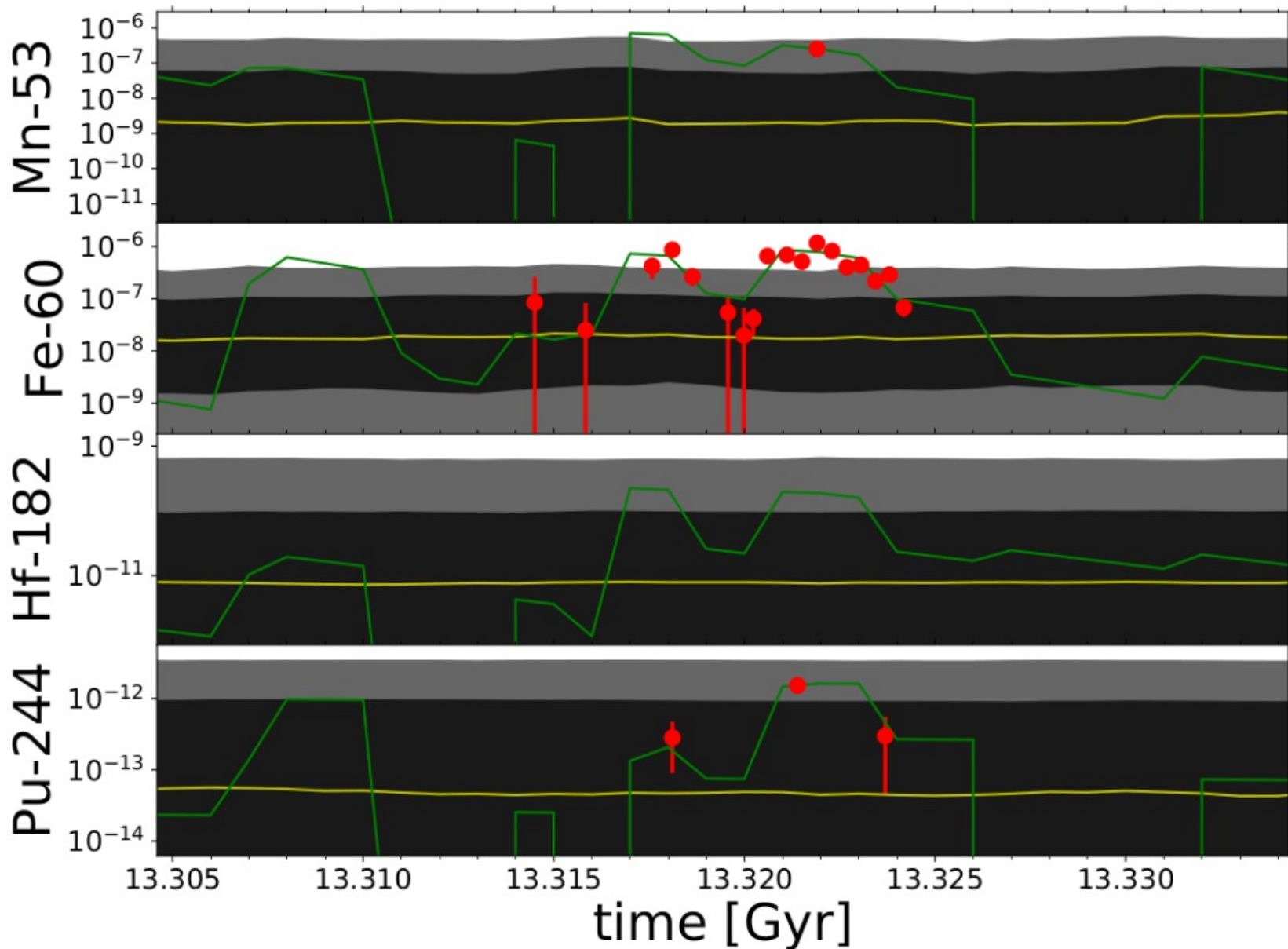
RESEARCH

NUCLEAR ASTROPHYSICS

^{60}Fe and ^{244}Pu deposited on Earth constrain the r-process yields of recent nearby supernovae

A. Wallner^{1,2*}, M. B. Froehlich¹, M. A. C. Hotchkis³, N. Kinoshita⁴, M. Paul⁵, M. Martschini^{1,†}, S. Pavetich¹, S. G. Tims¹, N. Kivel⁶, D. Schumann⁶, M. Honda^{7,‡}, H. Matsuzaki⁸, T. Yamagata⁸

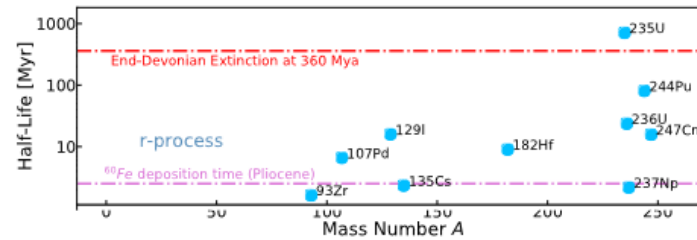
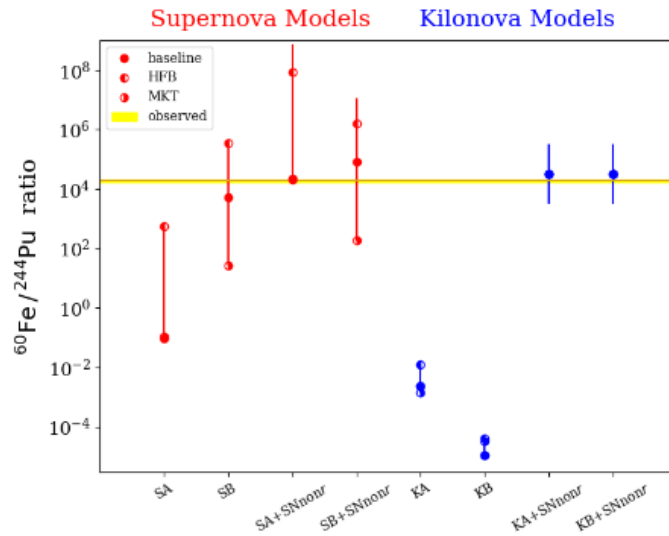
Compare 3D model to deep-sea detection values



Fe-60, Pu-244 from Wallner+, Mn-53 from Korschinek+, time shifted

Other possibilities of Fe-60 and Pu-244 sources as suggested by Rebecca this morning:





Actinide observables: ^{60}Fe and ^{244}Pu in Fe-Mn crusts



Wang, Clark, Ellis, Ertel, Fields, Fry, Liu, Miller, Surman, ApJ 2021;
 Wang, Clark, Ellis, Ertel, Fields, Fry, Liu, Miller, Surman, ApJ 2023



Core-collapse Supernova Explosions Driven by the Hadron-quark Phase Transition as a Rare r -process Site

Tobias Fischer¹ , Meng-Ru Wu^{2,3,4} , Benjamin Wehmeyer^{5,6}, Niels-Uwe F. Bastian¹, Gabriel Martínez-Pinedo^{7,8} , and Friedrich-Karl Thielemann^{7,9} 

¹ Institute of Theoretical Physics, University of Wrocław, 50-204 Wrocław, Poland; tobias.fischer@uwr.edu.pl

² Institute of Physics, Academia Sinica, Taipei, 11529, Taiwan; mwu@gate.sinica.edu.tw

³ Institute of Astronomy and Astrophysics, Academia Sinica, Taipei 10617, Taiwan

THE ASTROPHYSICAL JOURNAL, 894:9 (13pp), 2020 May 1

Fischer et al.

Table 3
Ejecta Properties of the Supernova Explosion Models

$M_{\text{prog}}^{\text{a}}$ (M_{\odot})	$M_{\text{inner ejecta}}^{\text{b}}$ ($10^{-2} M_{\odot}$)	$M_{\text{direct}}^{\text{c}}$ ($10^{-2} M_{\odot}$)	$M_{\text{intermediate}}^{\text{d}}$ ($10^{-3} M_{\odot}$)	$M_{\text{NDW}}^{\text{e}}$ ($10^{-3} M_{\odot}$)	M_{Fe}^{f} ($10^{-2} M_{\odot}$)	M_{Sr}^{f} ($10^{-4} M_{\odot}$)	M_{Eu}^{f} ($10^{-6} M_{\odot}$)	$M_{\text{244Pu}}^{\text{f,g}}$ ($10^{-10} M_{\odot}$)	$M_{\text{60Fe}}^{\text{h}}$ ($10^{-5} M_{\odot}$)
35†	1.44	1.03	3.72	0.33	7.15	6.50	7.86	2.09	12.2
40†	1.33	0.97	3.19	0.43	7.62	6.15	2.26	2.64	3.2
50‡	1.80	1.45	3.06	0.46	3.73	8.22	11.03	22.59	0.5

Notes. All yields are evaluated after about 1 Gyr.

^a ZAMS masses of the stellar models (same as in Table 2), †: Rauscher et al. (2002) and ‡: Umeda & Nomoto (2008).

^b Total inner ejecta mass launched from the PNS surface

See also yesterday's talk:

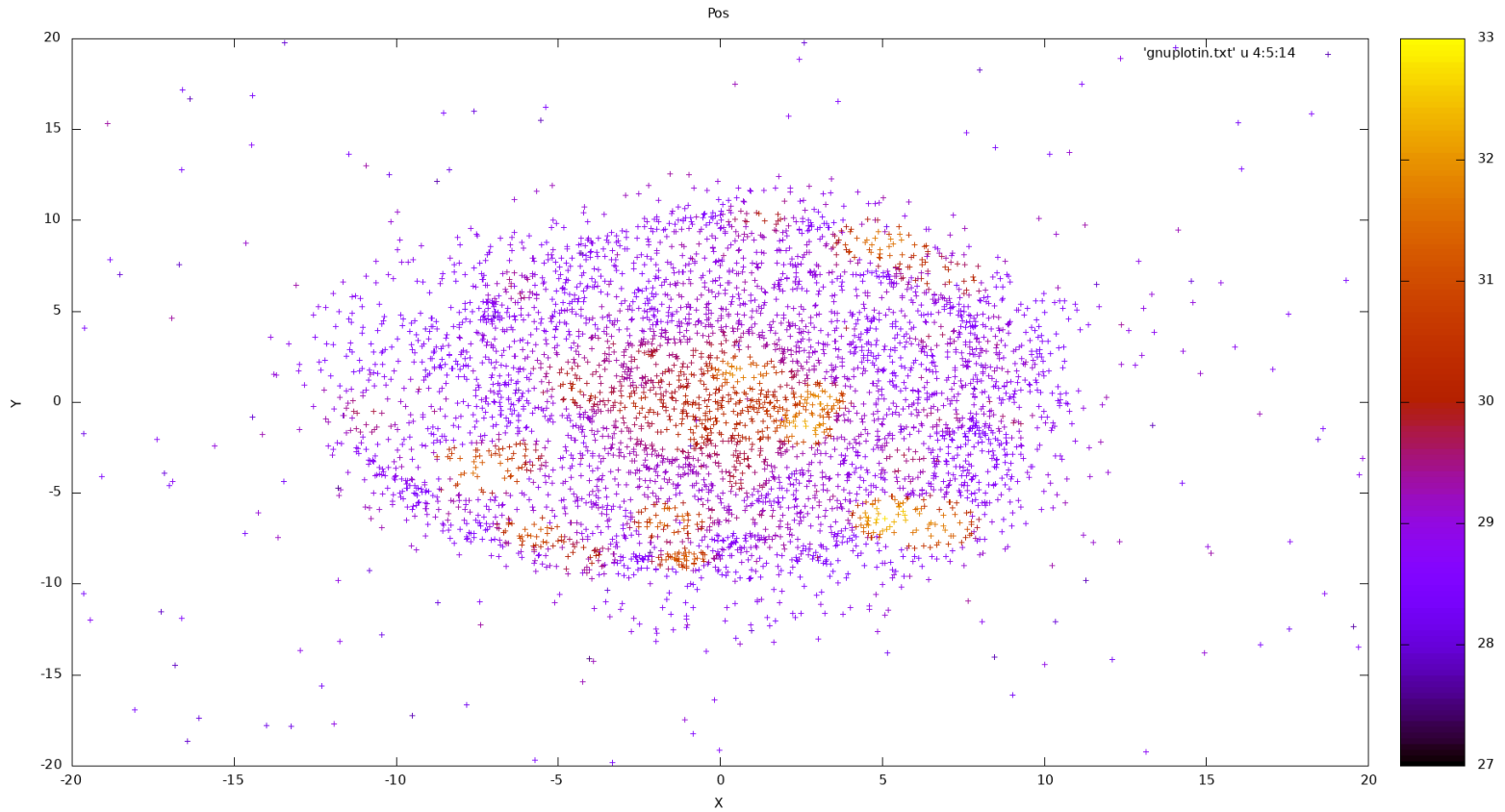
Constraining the onset density for the QCD phase transition with the supernova neutrino signal Noshad Khosravi Largani

Aula Grande, FBK Headquarters

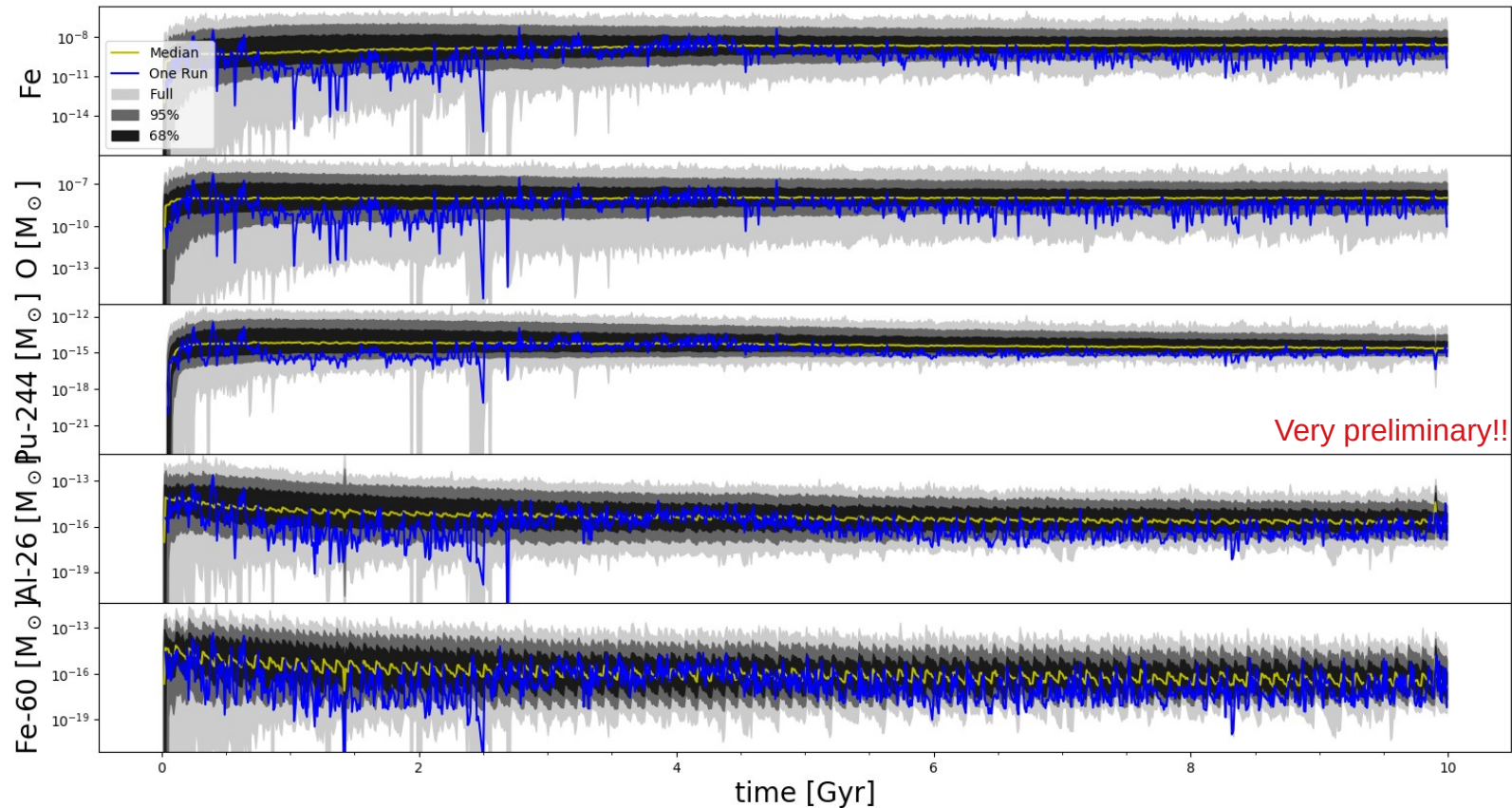
15:10 - 15:30

One step further: implementing SLRs in
Kobayashi **chemodynamical cosmological zoom-in SPH model**

One step further: implementing SLRs in Kobayashi chemodynamical cosmological zoom-in SPH model



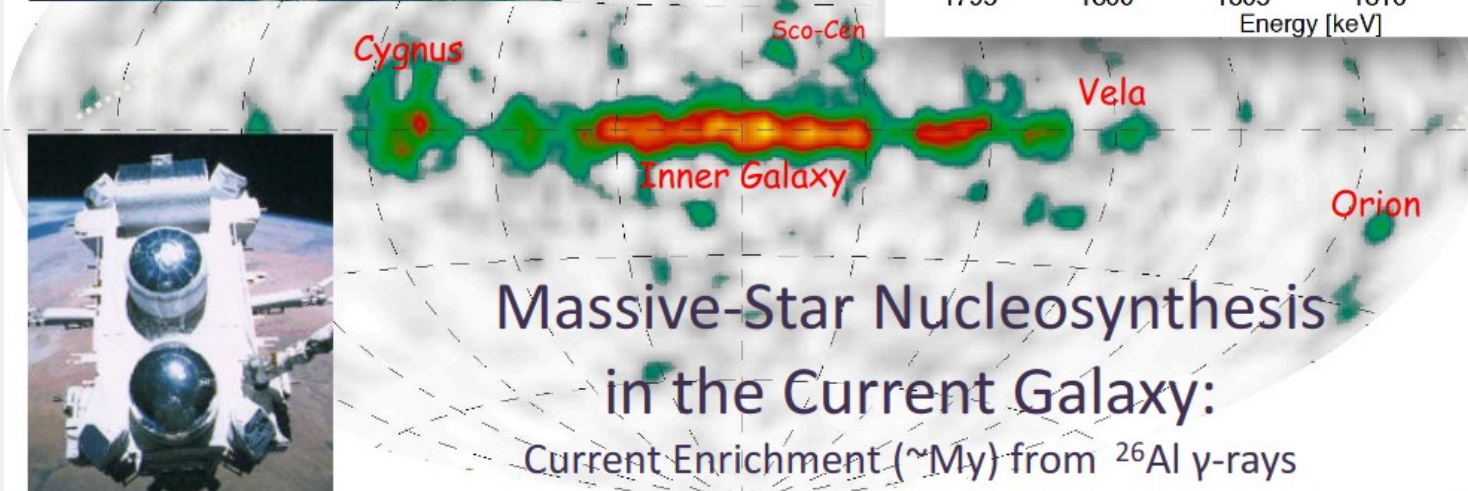
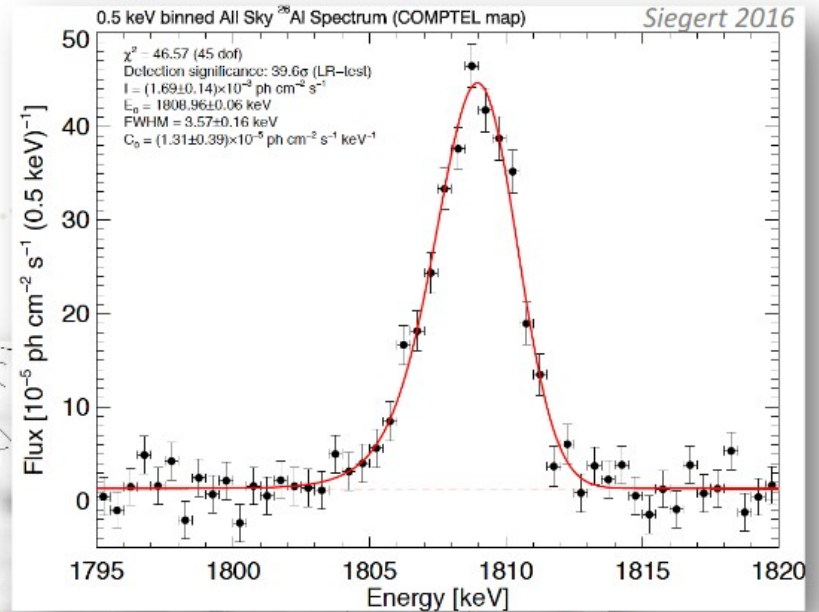
One step further: implementing SLRs in Kobayashi chemodynamical cosmological zoom-in SPH model



- Many features (DM, hydrodynamics, feedback) are included
- Know exactly where (spiral arms?) in the Galaxy and when which SLRs can be found

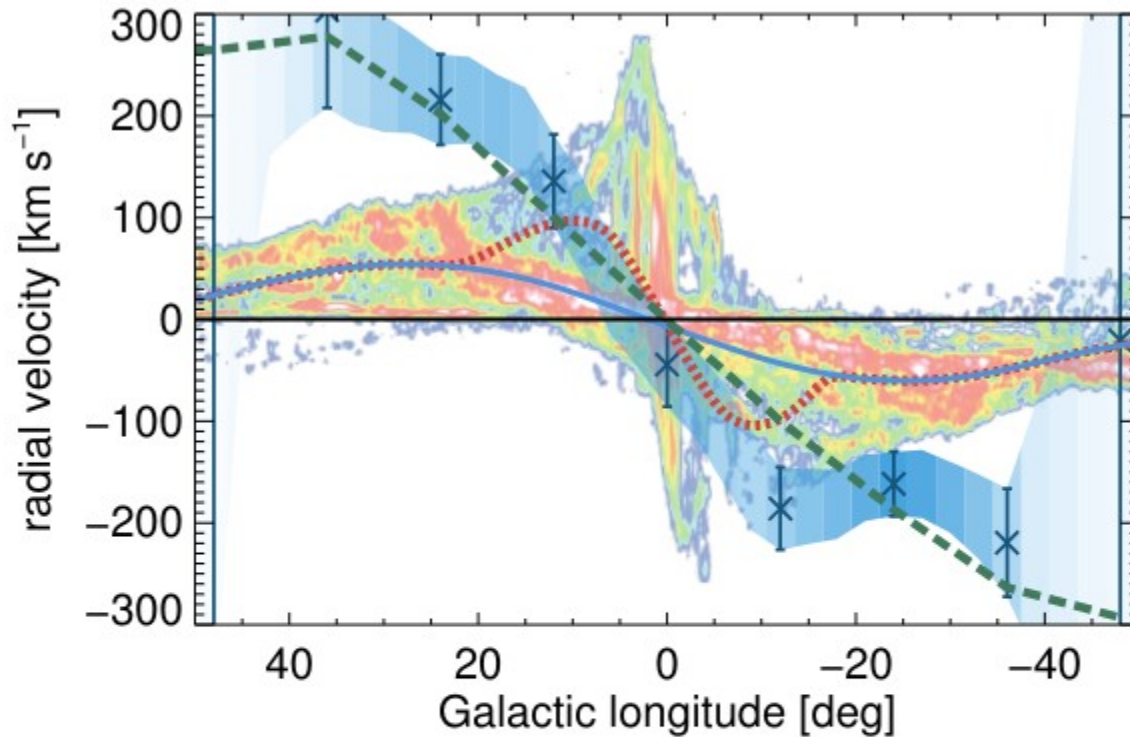
We can use current Al-26 emission to pinpoint stellar activity!

^{26}Al in our Galaxy: γ -ray Image and Spectrum



...Slide stolen from R. Diehl, see many talks this workshop

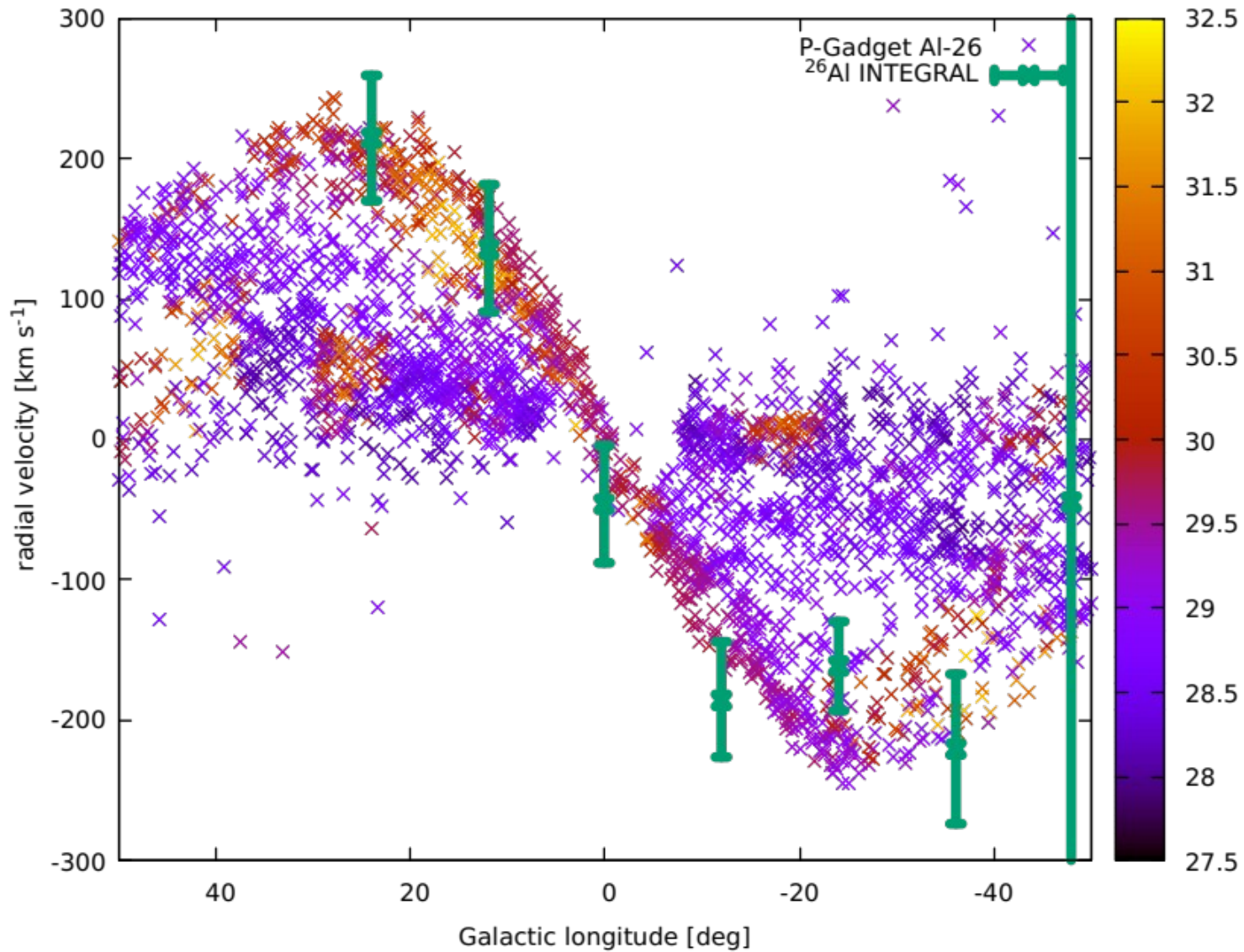
It will provide us with an “emission map” of the Galaxy:
We can interpret it using Galaxv models!



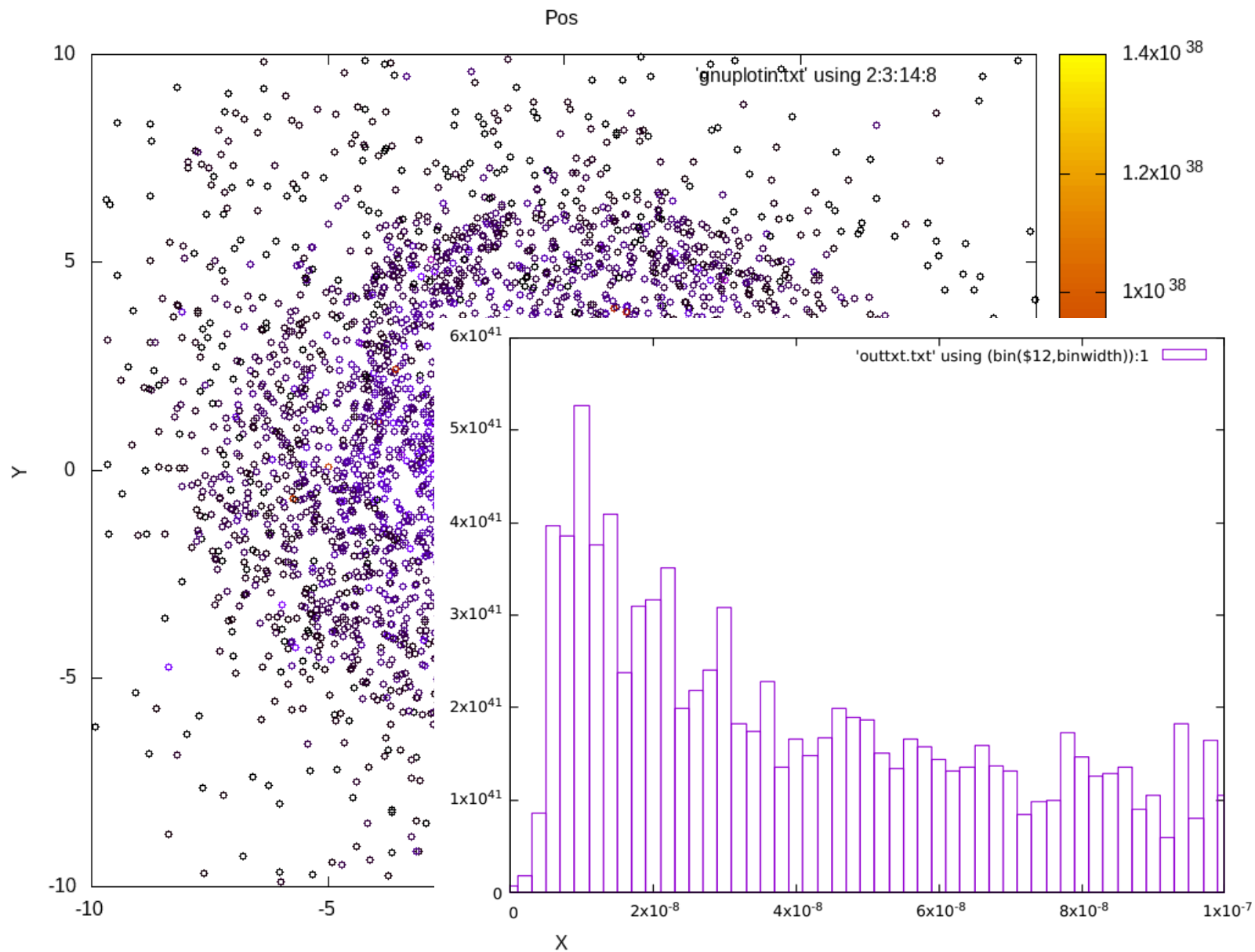
Kretschmer+13

Fig. 8. Longitude-velocity diagram comparing γ -ray-measured velocities (crosses, including error bars) with other objects in our Galaxy. ²⁶Al line-centroid energies were fitted to determine velocities in longitude bins of 12° and latitude ranges $\pm 5^\circ$. For comparison, different models are shown (blue solid, red dotted, and green dashed lines), as well as the velocity information from molecular gas seen in CO (see Sect. 4 for details).

It will provide us with an “emission map” of the Galaxy:
We can interpret it using Galaxy models!



This might also help to find Galactic areas with habitable planets!



With radioactive isotopes also heating planetesimals

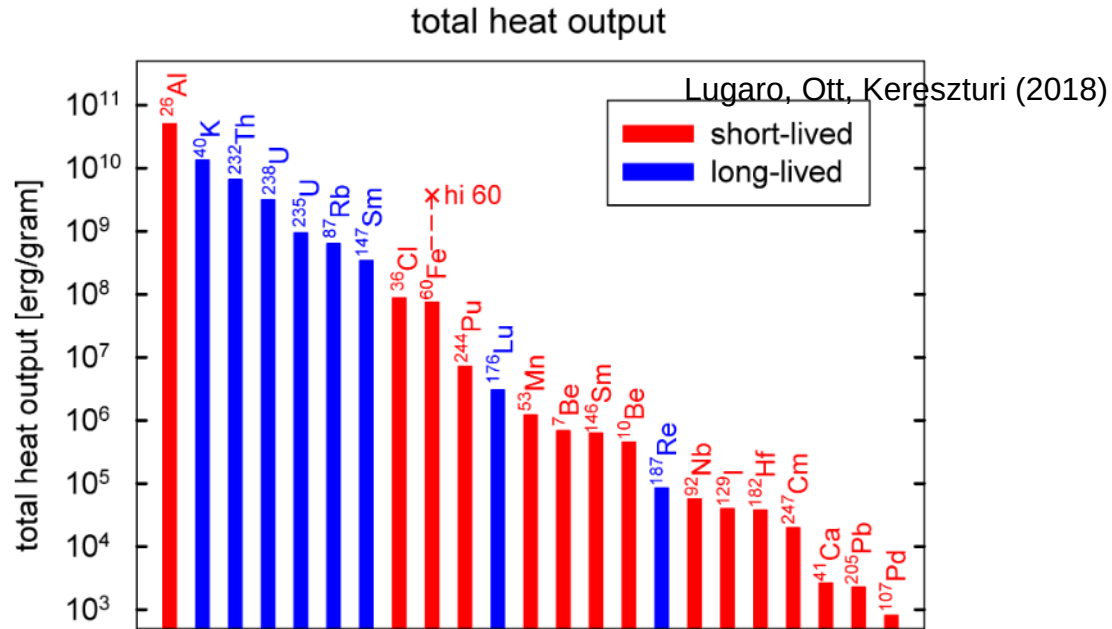


Figure 15: Total energy available for heating from radioactive decay per gram of material in the Solar System (CI meteorite composition) after the initially present isotope has completely decayed. For ¹⁰Be/⁹Be a value of 1×10^{-3} was used. For ⁶⁰Fe also the situation for a high abundance (⁶⁰Fe/⁵⁶Fe = 5×10^{-7} as compared to 1.01×10^{-8} given in Table 2) is indicated.

Conclusions

- We can constrain the SLR abundances and uncertainties by using the timing information of the sources (δ , γ), and vice versa
- SLRs may give us information about the nucleosynthesis conditions of the last event before formation of the Solar system
- SLRs seem to arrive on Earth simultaneously
 - This can be explained with the appropriate statistical tools
 - Can be further constrained by more deep-sea sediment detections
- Al-26 maps can help us locate stellar activity
 - This can be modeled with Galaxy evolution models
- We can identify regions in the Galaxy with enhanced isotope abundances
 - Might help to find areas with potentially habitable planets



We acknowledge support from the European Research Council under ERC Consolidator Grant Agreement No. 724560 “RADIOSTAR” (PI: Maria Lugaro), and the Swiss National Science Foundation (SNF). This work benefited from COST action ChETEC (16117) and support from the National Science Foundation Grant no. PHY-1430152 (JINA Center for the Evolution of the Elements), and Grant no. OISE-1927130 (IReNA).